https://doi.org/10.5194/egusphere-2026-247
Preprint. Discussion started: 3 February 2026

A new sediment budget for the Congo River Basin reveals underestimated tributary contributions and large-scale deposition

Nathan Carlier[1], Matti Barthel[2], Antoine de Clippele[2], Lissie W. de Groot[2], Travis W. Drake[2], Jordon D. Hemingway[3], Yi Hou[3], José Nlandu Wabakanghanzi[4], Joseph Zambo Mandea[5], Pengzhi Zhao[1], Johan Six[2], and Kristof Van Oost[1]

[1]Earth and Life Institute, Université Catholique de Louvain (UCLouvain), 1348 Louvain-la-Neuve, Belgium
[2]Department of Environmental Systems Sciences, ETH Zurich, 8092 Zurich, Switzerland
[3]Department of Earth and Planetary Sciences, ETH Zurich, 8092 Zurich, Switzerland
[4]Department of Soil Physics and Hydrology, Congo Atomic Energy Commission, Kinsahsa XI, Democratic Republic of Congo
[5]Woodwell Climate Research Center, Woods Hole, Falmouth, MA, United States

Correspondence: Nathan Carlier (nathan.carlier@uclouvain.be)

Abstract. Sediment yields from fluvial networks to the global oceans impact land carbon and nutrient cycles and are susceptible to climate, population, and vegetation changes. The Congo River Basin is a frontier for population and land use change, but sediment yield dynamics are poorly constrained within its basin, in particular within its largest tributary, the Kasaï River. To address this, we aimed to (1) introduce a spatially flexible methodology for estimating sediment yield from remote sensing monitoring, (2) establish a budget for the Congo and Kasaï river basins from both major and secondary tributaries, and (3) better constrain depositional losses of sediment during transit in the mainstem. A random forest model was calibrated on Landsat-8 spectral data, and total suspended sediment was accurately predicted (measured vs. predicted R^2 = 0.79), though predictions degraded in highly turbid waters due to spectral saturation. A sediment budget of the Congo River revealed that $33.0\,\mathrm{Tg\,yr^{-1}}$ are exported to the coastal ocean. Most sediment is derived from Congo River headwaters, the Kasaï River, the Oubangui River, and the Aruwimi River, whereas lower-order tributaries contributed 10% of all sediment inputs. Meanwhile, major contributors to the Kasaï budget (export = $11.1\,\mathrm{Tg\,yr^{-1}}$) were the Kasaï headwaters, Sankuru, and Kwango-Kwilu rivers. Finally, we found the Cuvette Centrale, a peatland-dominated depression, to be a depositional hotspot, and we estimated its net sediment deposition to be between $5.96\,\mathrm{Tg\,yr^{-1}}$ and $9.4\,\mathrm{Tg\,yr^{-1}}$. By monitoring Congo River Basin sediment transport, we aim to provide a better understanding of the Earth-surface processes occurring in a globally significant and rapidly changing watershed that lacks crucial baseline information on its sediment and carbon cycles.

1 Introduction

The movement of sediment through the land system involves multiple processes including soil erosion, mass wasting, channel erosion, and floodplain storage (de Vente and Poesen, 2005; de Vente et al., 2007). The complex dynamics of these processes are integrated into fluvial networks as sediment yield, which (per geomorphological convention) refers to the total mass of sediment exported from a catchment per unit time. Sediment export is tightly linked to the carbon balance, because sediments transport and transform carbon across the land–water continuum (Regnier et al., 2013; Van Oost and Six, 2023). As such, sediment yield is an indicator of the land's soil and water health, and carbon and nutrient balances (Lal, 2003; Syvitski et al., 2005). Sediment yield from global fluvial systems to the oceans is estimated at 17.3 (13.6-20) $\mathrm{Pg\,yr^{-1}}$ (Syvitski et al., 2022). Total export of carbon to the oceans is estimated to be 1.02 $\mathrm{Pg\,yr^{-1}}$ while particulate organic carbon (POC) is estimated to be exported at a rate of 0.18 $\mathrm{Pg\,yr^{-1}}$ and is associated with sediment dynamics (Ludwig et al., 1996; Liu et al., 2024). Sediment yield is controlled by multiple factors including lithology and geology, basin topography, vegetation, rainfall, and human impacts (Syvitski and Milliman, 2007). Moreover, anthropogenically induced erosion has increased global sediment yield by $\sim$200% (1950-2010), a major part of which is caused by agriculture, because erosion within croplands is on average 4 times faster than global erosion (Borrelli et al., 2017; Syvitski et al., 2005, 2022). While sediment yield has increased, anthropogenic impacts have decreased fluvial sediment delivery to the oceans (15.7 to 8.5 $\mathrm{Pg\,yr^{-1}}$ from 1950 to 2010) as building dams and reservoirs favors deposition within river networks (Syvitski and Milliman, 2007; Syvitski et al., 2022; Walling and Fang, 2003).

Despite these global trends, several areas remain understudied because in situ studies are both costly and difficult to implement. Of particular interest here is the Congo River Basin (CRB); it is the second largest basin in the world, draining a globally significant tropical forest (Xu et al., 2017) and extensive peatlands (Dargie et al., 2017), while being largely unimpacted by dams and reservoirs (Grill et al., 2019). Furthermore, it is undergoing a demographic explosion that is projected to increase the population five-fold within 100 years (United Nations Department of Economic and Social Affairs, 2024); this will drive a rapid land-use transition to agriculture, which in turn will increase soil erosion and is likely to substantially impact sediment yields. Assessing the future evolution of sediment dynamics (and consequently nutrient and carbon dynamics) in the CRB requires a quantified baseline understanding of different sediment transport pathways. We identified three key gaps in the current body of knowledge on sediment transport.

First, in contrast to sediment yield at the mouth of the CRB—which is well monitored since the 1980s (Moukandi N'kaya et al., 2020)—relatively little is known about the magnitude of particulate export from the diverse tropical landscapes within the interior of the CRB. Still, CRB sediment budgets have estimated contributions of three major Congo River tributaries (Kasaï, Oubangui, Sangha) from in situ monitoring data (Laraque et al., 2009; Coynel et al., 2005; Bouillon et al., 2014) and from a soil erosion model (Datok et al., 2021). Additional monitoring data reveals contributions from other tributaries such as the Ruki (Drake et al., 2023), the Aruwimi, and the Lomami rivers (Tshimanga et al., 2022). Moreover, sediment yield data is patchy and lacking in temporal consistency, both in duration and observation period. This lack of source-to-sink understanding of how various geomorphic processes operate on diverse landscapes within the basin hinders our ability to assess how future changes may affect sediment and carbon storage within the CRB.

Second, the Kasaï River Basin is virtually unstudied in terms of sediment yields (Laraque et al., 2009; Tshimanga et al., 2022) despite being the largest tributary of the Congo River and a frontier of anthropogenic impact (Center For International Earth Science Information Network, 2017; Hansen et al., 2013). Furthermore, thanks to its clear gradient of sediment yield drivers (i.e., land cover, human impact, and precipitation) and its simplified sediment transport dynamics (i.e., a single flood wave and no large depositional hotspot in the middle of its course), the Kasaï River provides an ideal study site for disentangling sediment yield controls in the African tropics.

Finally, there likely exist depositional hotspots along the sediment pathway of the Congo River mainstem. Two depositional hotspots have been proposed: first, a smaller hotspot at the widening of Malebo Pool near Kinshasa (proposed deposition rate of $2.53\,\mathrm{Tg\,yr^{-1}}$; Coynel et al., 2005) and second, a larger hotspot in the depression of the Cuvette Centrale (proposed deposition rate of $23\,\mathrm{Tg\,yr^{-1}}$; Datok et al., 2021). However, both studies' estimates of deposition are based on monitoring in the middle of the Cuvette Centrale (Ruki confluence with the Congo River), thereby missing a significant upstream chunk of river from a hypothesized major depositional hotspot.

Recent advances in remote sensing and machine learning models now allow spatially explicit estimates of sediment yield dynamics, bypassing many limitations of on-site monitoring. Visible and infrared spectra may be used to predict total suspended sediment (TSS) concentrations in water (Novo et al., 1989), which can be done from Earth-observation satellites using methods ranging from site-specific relationships (Doxaran et al., 2003) to regionally (Narayanan et al., 2024; Overeem et al., 2017) and globally applicable workflows (Dethier et al., 2020; Hou et al., 2024; Sun et al., 2025). TSS monitoring is an essential component in estimating fluvial sediment yields, and despite leaving out the bedload transport component of total sediment yield (generally assumed to be of low importance), sediment yield monitoring from remote sensing has successfully been applied to identify sedimentation hotspots (Li et al., 2024), to quantify anthropogenically driven sediment transport changes (Dethier et al., 2022), and to map sedimentary interactions between a river and its floodplain (Fassoni-Andrade and Paiva, 2019). Globally applicable models have been used to predict TSS at the Congo River outlet, but calibration data from the African continent is underrepresented, if present at all (e.g., Sun et al., 2025), and a regionally applicable model for the CRB has never been published.

To address the lack of unified, cohesive, long-term records of sediment transport in the CRB, we first aimed to leverage state-of-the-art techniques in remote sensing and machine learning to calibrate a region-specific predictive model of TSS. We then employed the predictive TSS model to investigate sources and sinks of sediment dynamics; we specifically expanded on an already existing but restrictive sediment budget for the Congo River and built the first ever budget for the regionally representative Kasaï River. Finally, we attempted to better constrain depositional sediment losses during mainstem transit, both in terms of location and deposition rates.

2 Materials and methods

2.1 Study area

The Congo River, located in Central Africa, has a discharge of approximately $1300\,\mathrm{km^3\,yr^{-1}}$ and a drainage basin area of $3.7 \times 10^6\,\mathrm{km^2}$. The discharge at the most downstream gauging station (Kinshasa) exhibits little seasonal and interannual variability because of alternating wet seasons in southern-hemisphere (e.g., Upper Congo, Kasaï) and northern-hemisphere (e.g., Oubangui, Sangha) tributaries (Fig. 1) (Laraque et al., 2009, 2013; Alsdorf et al., 2016; Mushi et al., 2022). The Congo River flows through varied geomorphological environments (Runge, 2007; Spencer et al., 2012), from the tectonically influenced Central African Rift in its headwaters and upper section, to a middle section dominated by gentle anastomosing morphology (from Kisangani to the exit of the Cuvette Centrale), and a lower, deeply incised section of cataracts after a widening (Malebo

https://doi.org/10.5194/egusphere-2026-247
Preprint. Discussion started: 3 February 2026

Pool) near Kinshasa. Mean precipitation in the CRB is $1511\,\mathrm{mm\,yr^{-1}}$ (Fick and Hijmans, 2017), while vegetation cover is 65% forest, 20% grassland, and 11% shrubland (Zanaga et al., 2022). High mean precipitation and flat terrain in the anastomosing region of the basin leads to the development of vast peatlands, which cover $0.17 \times 10^6\,\mathrm{km^2}$ (4.7% of the total CRB area) (Crezee et al., 2022) (Fig. 1).

The Kasaï River, located in the south of the CRB, has a discharge of $280\,\mathrm{km^3\,yr^{-1}}$, a drainage area of $0.9\,10^6\,\mathrm{km^2}$ and is the largest tributary of the Congo River (Laraque et al., 2009). It contributes approximately 25% of the CRB's drainage area and 22% of its discharge (Mushi et al., 2019). The Kasaï River's discharge is defined by a single seasonal peak, and its course is generally anastomosing or braided from its source in Angola to its confluence with the Congo River at Kwamouth (Fig. 1). The precipitation within the basin is $1520\,\mathrm{mm\,yr^{-1}}$ (Fick and Hijmans, 2017), and its vegetation cover is 64% forest (mainly in the North of the basin), 15% shrubland, and 33% grassland (Zanaga et al., 2022).

2.2 Calibration of a predictive model for TSS

2.2.1 In situ data

TSS monitoring data was compiled from multiple sources to create a spatially representative dataset for the CRB. Only surface samples were retained to homogenize sample collection schemes. The first dataset came from a cruise sampling expedition along the Congo mainstem and its tributaries (2013-2015) which yielded 221 TSS samples (Lambert et al., 2016). A second dataset came from a monitoring campaign of the Ruki River, with 27 data points which were collected between 2019 and 2020 (Drake et al., 2023). Finally, 161 samples from a Congo River monitoring station in Kisangani were collected by the Centre de Surveillance de la Biodiviersité (CSB, Université de Kisangani) from 2012 to 2019.

2.2.2 Satellite data

Landsat-8 (L8) surface reflectance (Tier 1) was retrieved with Google Earth Engine (GEE). Spectral bands were selected from the visible spectrum (red, green, blue), near infrared (NIR), and short-wave infrared (SWIR) 1 & 2 (Gorelick et al., 2017). The shape of the spectral curve was also computed from normalized differences of each band combination. Using L8 image metadata, images were only retained if cloud cover < 85%, and cloud and cloud shadow pixels were masked out. Non-water pixels were also masked out using a normalized difference water index (NDWI) (McFeeters, 1996) with a threshold of -0.1 (i.e., NDWI > -0.1 is considered water) (Fig. 2a). Median reflectance for each band was then extracted for each in situ data point, with a buffer (500 m or 100 m for large and small rivers respectively) around each point.

To ensure a high-quality dataset suitable for model calibration and validation, strict filtering steps were applied to the in situ TSS observations prior to analysis. First, 40 observations (from smaller-order tributaries) could not be spatially resolved due to the coarse resolution of L8. Second, a maximum time window of 11 days (Fig. A1) for matches between in situ observations and their closest L8 image was allowed. Thus, 149 observations were removed as they lacked an L8 image match due to persistent cloud cover over the tropics (Potapov et al., 2012). Third, 3 observations with high TSS were removed (a priori threshold of TSS > $100\,\mathrm{mg\,L^{-1}}$) due to spectral saturation within highly turbid waters (see below for further discussion) (Balasubramanian et al., 2020; Han et al., 2016). Finally, 2 observations displayed abnormally high residuals following model calibration (see Section 2.2.4) and were thus removed. The final dataset comprised 184 observations (i.e., 45% of the original dataset) of which 86 points were published by Lambert et al. (2016), 12 points by Drake et al. (2023), and the last 86 points from the CSB's monitoring efforts (Fig. A2).

2.2.3 Contextual covariables

Contextual covariables were added to the spectral variables in the model calibration (Fig. 2) to help negate the effects of confounding factors (e.g., mineralogy, grain size distribution, chlorophyll-a) (Dethier et al., 2020; Sagan et al., 2020). Contextual covariables include: latitude and longitude of the in situ observation, Euclidean distance from the Congo River's outlet, discharge on the day of the in situ observation (Wongchuig et al., 2023), average silt content (Poggio et al., 2021) from the major subbasins (level 4 of HydroBASINs; Lehner and Grill, 2013) of the Congo River, day number of the year of in situ observation, and 6 binary variables for the river Strahler order (one variable per order number from 4 to 9).

2.2.4 Model calibration, validation, errors

The following analyses were performed in the R statistical computing environment (v 4.3.3; R Core Team, 2024), leveraging the libraries *caret* (Kuhn, 2008) and *ranger* (Wright and Ziegler, 2017). The dataset was randomly partitioned into 2 parts. The first part (hereafter termed "training dataset"), which contained 80% of all in situ data (n = 148; mean = 33.6 $\mathrm{mg\,L^{-1}}$; standard deviation = 22.7 $\mathrm{mg\,L^{-1}}$), was used for model calibration. The remaining 20% of all in situ data (n = 36; mean = 33.0 $\mathrm{mg\,L^{-1}}$; standard deviation = 21.9 $\mathrm{mg\,L^{-1}}$) were used for independent model validation (hereafter termed "independent validation dataset").

For analysis, training data were first normalized by subtracting its mean and dividing by standard deviation. Then, a random forest (RF) regression algorithm was selected as the best performing algorithm for predicting TSS (Section A2) thanks to its effectiveness with non-linear relationships and interaction effects between predictive variables (Cutler et al., 2007). Hyperparameter tuning of the random forest (using a default 500 trees) was conducted in *caret*, and the best combination of hyperparameters was selected as that which minimizes root mean square error (RMSE). Model performance was evaluated using the proportion of total variation of predicted values explained by the model (R^2), mean absolute error (MAE), RMSE, relative error (%) (Dethier et al., 2020), and % bias defined as

$$Bias = \frac{\sum_{i=1}^{N}(TSS_{pred,i} - TSS_{obs,i})}{\sum_{i=1}^{N} TSS_{obs,i}} \times 100\%, \tag{1}$$

where TSS_{pred} is predicted TSS, TSS_{obs} is in situ observed TSS, and N is the size of the dataset. Performance was cross-validated with 5 repetitions of a 10-fold cross-validation, and standard error of predictions was computed from infinitesimal jackknifing (Wager et al., 2014).

Resulting RF model complexity was then optimized with the recursive feature elimination (RFE) algorithm, in which new RF models were calibrated with subsets of variables (5, 10, 15, and 20) selected based on their importance from the previous step's RF model. The RFE algorithm prioritized model simplicity at a minimal cost of performance by selecting the model which contained the smallest number of variables while remaining within 2% of the original RF model's RMSE.

Finally, performance of the TSS predictive model was assessed using the metrics defined above (R^2, MAE, RMSE, relative error, and % bias) between in situ observations and predicted TSS of the independent validation dataset.

2.3 Sediment budgets of the Congo and Kasaï

Ten major tributaries were selected as inputs of the Congo River sediment budget (Fig. 1), for which "virtual" monitoring stations were placed near their confluence with the Congo River. A single output, downstream of all inputs and along the Congo River's mainstem, was placed near Kinshasa (hereafter named Congo-Kinshasa) to match previous monitoring records (Laraque et al., 2009; Spencer et al., 2012; Hemingway et al., 2017). For the Kasaï River sediment budget, 7 major tributaries were identified and selected as inputs, whereas the confluence of the Kasaï River with the Congo River was selected as the output. TSS was predicted for the satellite time series (2015-2019) at each virtual monitoring station using our calibrated RF model (satellite data was collected using the same methodology as in Section 2.2.2).

2.3.1 From TSS to sediment yield

Predicted TSS concentrations were temporally interpolated to obtain daily predictions (assuming TSS concentrations exhibit low weekly to monthly variability) and converted to daily yields as

$$SY_{daily} = Q \times TSS_{pred} \times (8.64 \times 10^{-8}), \tag{2}$$

where Q ($\mathrm{m^3\,s^{-1}}$) is daily discharge obtained from Wongchuig et al. (2023), SY_{daily} is daily sediment yield ($\mathrm{Tg\,day^{-1}}$), and the last numerical term is a unit conversion factor. Daily sediment yields were then summed to obtain yearly sediment yields ($\mathrm{Tg\,yr^{-1}}$). Coefficients of variation (CVs) (the quotient of mean sediment yield of each virtual station to its corresponding standard deviation) were computed to investigate intra- and inter-annual variations of sediment yield. Intra-annual CVs were computed as

$$CV_{intra} = \frac{1}{n}\sum_{i=1}^{N}\frac{SYdaily_{\sigma,i}}{SYdaily_{\mu,i}}, \tag{3}$$

where CV_{intra} is intra-annual CV, n is the observation time window (i.e., 5 years from 2015 to 2019), $SYdaily_{\sigma,i}$ is the standard deviation of daily sediment yield for an individual year, and $SYdaily_{\mu,i}$ is the average daily sediment yield for an individual year. Furthermore, inter-annual CVs were computed as

$$CV_{inter} = \frac{SYyearly_{\sigma}}{SYyearly_{\mu}}, \tag{4}$$

where CV_{inter} is inter-annual CV, $SYyearly_{\sigma}$ is the standard deviation of yearly sediment yield (2015-2019) and $SYyearly_{\mu}$ is the mean yearly sediment yield for the same observation period. Finally, yearly trends were statistically tested for monotonic increasing or decreasing patterns using a Mann-Kendall test (Libiseller and Grimvall, 2002).

Finally, a 95% confidence interval (CI) for TSS predictions was computed from predicted standard errors (Section 2.2.4), and discharge CIs were simulated following the method described in Section A3.

2.4 Estimating sediment deposition within the Cuvette Centrale

Two approaches were used to estimate sediment accumulation rates within the Cuvette Centrale. First, using the sediment budget of the Congo River (Section 2.3), a sediment balance showed net sediment yield differences between the output (Congo-Kinshasa) and all the inputs (upstream Congo and all tributaries). A deficit of sediment yield at the output compared to inputs was considered as net accumulation/deposition during transit. In the second approach, virtual monitoring stations were set up every 10 km on a transect along the mainstem of the Congo River from headwaters to the outlet. Yearly sediment yields were computed for each virtual monitoring station (Section 2.3), and changes in sediment yields along the transect could then be interpreted as net gains or losses.

3 Results

3.1 Predictions of total suspended sediment

3.1.1 Random forest model calibration and validation

RF model performance was improved by including contextual covariables and by the RFE variable reduction algorithm (Table 1), leading to RMSE = $11.5\,\mathrm{mg\,L^{-1}}$, MAE = $8.61\,\mathrm{mg\,L^{-1}}$, and $R^2 = 0.76$ from the training dataset. In total, 15 variables were retained by the RFE algorithm (out of 33 spectral and contextual variables). Ten variables were satellite derived, with variables involving visible bands (unique spectral bands and normalized differences) exhibiting a high model importance (Fig. A3), and five variables were contextual (discharge, day number of the year, longitude, Euclidean distance to Congo outlet, and Strahler order 8).

3.1.2 TSS predictions of the major subbasins of the Congo and Kasaï Rivers

Our predicted TSS time series (2015-2019) exhibit values ranging from a minimum of $2.72\,\mathrm{mg\,L^{-1}}$ (outlet of the Lulonga River) to a maximum of $66.4\,\mathrm{mg\,L^{-1}}$ (Congo River). Between the Congo River stations of Kisangani (Congo headwaters) and Kinshasa (near the outlet), mean TSS declined from 42.8 to $25.6\,\mathrm{mg\,L^{-1}}$, a 40% decrease. A 19% decrease was also observed between the Kasaï River upstream station and the outlet. Subbasins exhibiting extreme TSS values (i.e., TSS $< 10\,\mathrm{mg\,L^{-1}}$ and TSS $> 40\,\mathrm{mg\,L^{-1}}$) tended to display narrower distributions (standard deviation $< 4.5\,\mathrm{mg\,L^{-1}}$) than subbasins with intermediate TSS values (average standard deviation = $7.9\,\mathrm{mg\,L^{-1}}$) (Fig. 3), with the exception of the Aruwimi River and Congo headwaters (i.e., high TSS but high standard deviation).

In addition to predicting TSS time series in virtual stations, predictions can also be performed over open waters in the CRB, in a gridded format. We compiled composite images of spectral variables by taking median values from a 3-year collection (2018-2020) of images from Kinshasa's wet season (September to April) and applying our predictive model over the resulting grid (a small part of the CRB was chosen for visualization purposes). The gridded range of TSS predictions for the Congo-Kasaï confluence was 2-66 $\mathrm{mg\,L^{-1}}$ (Fig. 4). Furthermore, high cross-sectional variability could be observed within rivers, such as the braided river section of the Congo River, or downstream of confluences such as Kwango-Kwilu, Kwango-Kasaï, and Kasaï-Fimi.

3.2 Sediment spatio-temporal dynamics of the Congo and Kasaï

3.2.1 Sediment budgets

Average yearly sediment yield for the Congo River in the years 2015-2019 was 33.0 $\mathrm{Tg\,yr^{-1}}$ at the Congo-Kinshasa station. Main contributors to this budget were from the mainstem (Congo headwaters) with 51% of inputs, as well as the Kasaï (34%), Oubangui (13%), and Aruwimi rivers (11%) (Fig. 5a). The combined contribution of all other tributaries represented 10% of total inputs. Over the same time period, the average sediment yield for the Kasaï River at its outlet was 11.1 $\mathrm{Tg\,yr^{-1}}$, with major contributions from the Kasaï mainstem headwaters (28%), the Sankuru (17%), and the Kwango-Kwilu (32%) rivers. Other tributaries contributed 14% of the total input (Fig. 5b).

3.2.2 Seasonal and annual variability

For most CRB river basins, intra-annual sediment yield cycled seasonally between low and high values due to wet- and dry-season cycles (Fig. 6). Intra-annual coefficients of variations (CVs) ranged from 0.21 to 0.88, with the lowest CV occurring at the Congo-Kinshasa station and the highest CV occurring in the Oubangui River. Meanwhile, inter-annual CV ranged from a minimum of 0.06 in the Aruwimi and Lwange rivers to a maximum of 0.2 in multiple rivers (Fig. 7). Two rivers (Lulua and Lomami) both displayed a significant monotonic positive trend (Mann-Kendall test) from 2015 to 2019, whereas all other rivers did not display any statistically significant trend.

3.3 Deposition rates within the Cuvette Centrale

3.3.1 Sediment budget balance

Congo River sediment budget results (Fig. 5) indicate that inputs exceeded outputs. Specifically, we observed a mass-balance sediment deficit of 5.96 $\mathrm{Tg\,yr^{-1}}$ (CI = -5.6, 18), representing 15% of all inputs. In contrast, a sediment balance for the Kasaï River showed that an extra 8% (0.916 $\mathrm{Tg\,yr^{-1}}$, CI = -4.2, 6.1) of sediment was exported by the system compared to its inputs.

3.3.2 Sediment yield evolution along a transect

Predicted sediment yield at the most upstream point of the Congo River (i.e., ∼2900 km from the outlet) was 1.60 $\mathrm{Tg\,yr^{-1}}$ (CI = 1.2, 2.0); this slowly increased over 600 km of transit, reaching 5.57 $\mathrm{Tg\,yr^{-1}}$ (CI = 3.6, 7.6) just before the confluence with the Lowa River (Fig. 8). Sediment yield jumped to 11.8 $\mathrm{Tg\,yr^{-1}}$ (CI = 8.1, 15) due to contributions from the Lowa River, then remained relatively stable until reaching Kisangani (∼2100 km from outlet). After Kisangani, where the Congo River becomes more braided (Runge, 2007), sediment yield, as well as spatial variability, began to increase further. Past the confluence with the Aruwimi River (∼1800 km from outlet), sediment yields plateaued near 20.2 $\mathrm{Tg\,yr^{-1}}$ (CI = 16, 25) before beginning to decrease near the onset of the Cuvette Centrale (∼1600 km from outlet). From there, sediment yields further decreased to a local minimum of 10.8 $\mathrm{Tg\,yr^{-1}}$ (CI = 6.0, 16; ∼1100 km from outlet) before rebounding to 26.1 $\mathrm{Tg\,yr^{-1}}$ (CI = 19, 33) due to inputs from the Oubangui, Sangha, and Kasaï rivers (900-600 km from outlet). This increase was accompanied by a marked increase in spatial variability. Between the Kasaï River confluence and Kinshasa (∼400 km from outlet), sediment yield increased and spatial variability decreased, as the geomorphological regime of the mainstem transitions from anastomosing to meandering. The final section of the Congo River, downstream of Kinshasa, is characterized by waterfalls and rapids (Runge, 2007); sediment yield again plateaued in this region, although spatial variability increased drastically (Fig. 8).

4 Discussion

4.1 RF model performance

Challenges when building a predictive model for the CRB included regionally variable confounding factors (e.g., grain size distribution, mineralogy, sediment color, clorohpyll-*a*) (Dethier et al., 2020; Sagan et al., 2020) and the fact that our in situ TSS dataset is significantly smaller than that used in similar published works. For example, previous studies (Gardner et al., 2023; Li et al., 2024; Narayanan et al., 2024) used upwards of 1000–10,000 calibration samples for the Mississippi Basin, the Tibetan Plateau, and the Amazon Basin. Nevertheless, our model achieved similar predictive accuracy as others when quantified using regression R^2 values (i.e., R^2 = 0.73 in this study; R^2 = 0.62-0.94 in previous studies) (Park and Latrubesse, 2014; Fassoni-Andrade and Paiva, 2019; Pereira et al., 2018; Peterson et al., 2018; Wang et al., 2009; Sun et al., 2025). Such results have been observed previously; for example, both Overeem et al. (2017) and Yepez et al. (2017) similarly achieved high accuracy (R^2 = 0.9) despite using smaller datasets (i.e., 300 training samples). However, in contrast to our dataset from throughout the basin, those studies extrapolated their models from 1-3 monitoring stations to entire regions, which can introduce bias due to lack of spatial representativity.

Despite high accuracy, our model was subject to spectral saturation while predicting TSS, which involves the degradation of correlation between highly turbid waters and surface reflectance (Balasubramanian et al., 2020; Han et al., 2016). We first hypothesized that TSS > 100 $\mathrm{mg,\,L^{-1}}$ would suffer from spectral saturation, so observations above this threshold were removed a priori (Section 2.2.2). However, error assessment on our predictive model (Fig.2) revealed a heteroskedasticity at TSS $\geq$ 70 $\mathrm{mg,\,L^{-1}}$, which we interpreted as spectral saturation. Moreover, while this spectral saturation threshold may hold

https://doi.org/10.5194/egusphere-2026-247
Preprint. Discussion started: 3 February 2026

true for the Congo mainstem, abnormally low TSS prediction standard deviations were observed in the Lwange River and Kasaï headwaters despite TSS values near 45 mg, L^{-1} (Fig. 3); this may be evidence for a lower saturation threshold in the Kasaï River Basin and/or smaller-order rivers. While previous studies have managed to mitigate spectral saturation (Martinez et al., 2015; Novoa et al., 2017; Balasubramanian et al., 2020; Dethier et al., 2019, 2020), our RF model strongly relies on variables involving visible color (Fig. A3), and the model's response (i.e., the change in predictions in reaction to a variable's variation) is low in large zones of some spectral variables' ranges (Fig. A4), meaning that variations in reflectance do not lead to a change in predictions from the model. The hypothesized presence of two spectral saturation thresholds (i.e., 70 and 45 mg, L^{-1} for the Congo and its tributaries, respectively) is symptomatic of an underrepresentation of highly turbid conditions in the calibration data, especially in tributaries of the CRB.

Beyond spectral saturation, persistent cloud cover over the CRB (Potapov et al., 2012) hindered our ability to match in situ observations to L8 observations, thus reducing the training dataset size. To mitigate this, a large time window between L8 and in situ observations (11 days) and a wide buffer (500 m) were used when possible. These mitigation strategies represent a compromise, since within-river temporal and spatial variability may introduce errors in TSS predictions. However, a higher buffer size has previously been shown to increase model performance (Dethier et al., 2020) and temporal TSS variability is low in the CRB (Coynel et al., 2005). A final potential prediction bias could derive from the exclusive retention of surface samples in our in situ TSS dataset (i.e., depth samples were excluded for data consistency); indeed, depth-integrated TSS may change results (Laraque et al., 2009; Coynel et al., 2005). While a site-specific correction exists for the Kinshasa monitoring station (Moukandi N'kaya et al., 2020), this was not scaled to the entire CRB as this would likely add large, unconstrained errors.

4.2 Sediment budgets of the Congo and Kasaï rivers

Sediment yield errors are attributable to both TSS prediction errors (as described in Section 4.1) and the discharge product (Wongchuig et al., 2023). Indeed, discharge is estimated by a physically constrained model which has higher uncertainties than in situ discharge data, thus propagated to sediment yield estimates. However, this higher uncertainty was compensated by the product's applicability to a large array of rivers in the CRB, a long observation time scale, and high performance compared to worldwide products.

Sediment yield at the Congo-Kinshasa virtual station during the 2015-2019 period was predicted to be 33.0 $\mathrm{Tg\,yr^{-1}}$, which was broadly consistent with previously reported values (29–47 $\mathrm{Tg\,yr^{-1}}$; Table 2). In contrast, substantial discrepancies were observed for the Oubangui River, where our prediction was systematically higher than prior estimates. This bias is likely caused by an inconsistency in monitoring station location as our virtual station (near the outlet) is 550 km downstream of the in situ monitoring station in Bangui; most basins are not monitored in situ at the confluence with the main stem, which leads to mass-balance uncertainty. In contrast, our study provides the first estimates of sediment yields for regionally significant tributaries based on a consistent methodology and frequent sampling of TSS at each station.

Inter-annual trends revealed no change in sediment yield between 2015 and 2019 (except in the smaller-order rivers of Lulua and Lomami rivers), which could only be verified from a published 30-year analysis of the Congo-Kinshasa station (Moukandi N'kaya et al., 2020). For CRB tributaries, no comparable measurement could be found. The inter-annual variability of sediment yields which we observed is probably attributable to differing precipitation patterns between years, as a 5-year time window of observation is too short to observe anthropogenically driven changes in sediment yield (Dethier et al., 2022; Li et al., 2024). Moreover, any temporal changes in erosion that may be occurring within the studied basins over this period is likely muted due to their large catchment areas (Walling, 1983).

4.3 Deposition rates in the Cuvette Centrale

Our Congo River sediment budget analysis (Fig. 5) reveals that inputs exceed outputs, implying a substantial net deposition along the mainstem. Despite this difference not being significantly different to 0 in the overall sediment budget (5.96 $\mathrm{Tg\,yr^{-1}}$; CI = -5.6, 18), the sediment yield transect (Fig.8) displays statistically significant deposition (9.40 $\mathrm{Tg\,yr^{-1}}$; CI = 3.0, 16) within the Cuvette Centrale, a long flat stretch of anastomosing river, where reduced stream power limits sediment transport capacity and promotes deposition in the river channel (Runge, 2007). Moreover, lateral incursions of water into floodplains during the high-flow season may also contribute to trapping sediment (Georgiou et al., 2023).

Both deposition rates (5.96 and 9.40 $\mathrm{Tg\,yr^{-1}}$) calculated here are higher than a previous sediment budget balance estimate, where deposition rates were estimated at 2.53 $\mathrm{Tg\,yr^{-1}}$ (Coynel et al., 2005). However, a key methodological difference is the location of the "upstream Congo" station (i.e, the onset of net deposition), as Coynel et al. (2005) assumed this to be near the confluence of the Ruki River with the Congo River, 550 km downstream of the onset of sediment yield decrease in our model. In contrast, an erosion modelling approach estimated 23 $\mathrm{Tg\,yr^{-1}}$ of deposition in the Cuvette Centrale (Datok et al., 2021), roughly double the values calculated here. This higher estimate seems to be linked again to methodological differences, as Datok et al. (2021) estimated deposition rates within the entire river network, whereas our computation only considers net losses along the mainstem. Additionally, a large discrepancy between the sediment yield estimates at the Cuvette Centrale exit reported in Datok et al. (2021) (7.6 $\mathrm{Tg\,yr^{-1}}$) and in this study (15.4 $\mathrm{Tg\,yr^{-1}}$) may further contribute to explaining this offset in net depositional flux.

In contrast to the Congo River, our results indicate that the Kasaï River experiences no large-scale net deposition, as evidenced by the minor differences between modelled inputs and outputs (Fig. 5). Indeed, we see a small net increase in yields from inputs to outputs, although this value is not significantly different from 0. However, we may be underestimating inputs due to spectral saturation in some turbid rivers (e.g., Kasaï headwaters, Kwango, and Lwange rivers). Thus, any increase (if indeed present) could come from smaller tributaries or bank erosion (Langhorst and Pavelsky, 2023).

Sediment budget balances for both the Congo and Kasaï rivers provide information regarding net deposition as opposed to total/gross deposition. Indeed, concurrent processes of channel and floodplain deposition with other processes (e.g., bank erosion) serve to mask internal sediment dynamics of fluvial systems (Walling, 1999). A more in-depth look into the sediment budget and processes would require field-based investigations such as sedimentary records sampling.

4.4 Perspectives

Our methodology could be adapted to extend to other satellites, such as the Enhanced Thematic Mapper (ETM) aboard Landsat 5 and 7, which would increase the temporal coverage of TSS monitoring to 40 years (1984 onwards), assuming reasonable cloud pollution and a locally adapted spectral matching between sensors. The combination of satellites would permit a more thorough study of the temporal evolution of sediment yields within the basin. Additionally, smaller basins across the CRB and Kasaï River Basin could be investigated as erosional drivers of sediment yields could be more easily separated, thanks to clearly defined gradients of these basins.

The prediction of TSS was most hindered by the lack of data within the CRB. Especially for highly turbid rivers, spectral saturation prevented us from accurately predicting some lower-order tributaries. Nevertheless, spectral saturation was a minor problem for the present study, since major tributaries of the CRB tended to exhibit lower TSS concentrations. However, through the integration of local data to global datasets, accuracy could potentially be increased, and highly turbid rivers could be investigated (Dethier et al., 2020).

Finally, evidence shows that both particulate and dissolved organic carbon (POC, DOC) can be predicted from surface reflectance (Liu et al., 2019; Cao et al., 2018; Tian et al., 2025). The literature remains scarcer for remote sensing of OC compared to TSS (Topp et al., 2020) due to the relationship between OC and surface reflectance being less direct. However, a successfully calibrated model for POC and DOC would lead to a better understanding and OC budgets and transport pathways in the CRB.

5 Conclusions

Using a well-performing TSS prediction model (R^2 = 0.73), we generated a new sediment budget for the understudied CRB. We updated a previous budget that only considered the main tributaries (i.e., Oubangui, Sangha, Kasaï) by adding 6 new inputs from smaller tributaries; these accounted for 17% of the total $33.0\,\mathrm{Tg\,yr^{-1}}$ sediment yield at the Congo-Kinshasa station. We additionally generated the first-ever sediment budget for the Kasaï Basin (sediment yield of $11.1\,\mathrm{Tg\,yr^{-1}}$ at its outlet), including 6 major tributaries, of which the Kwango-Kwilu, Sankuru, and the Kasaï headwaters were the largest contributors. Seasonal and interannual variations were also computed for each river, displaying yearly sediment yield stability for most rivers, along with a marked diversity in seasonality between rivers. These results provided previously unknown information for many of the Congo River's tributaries.

By studying sediment processes within the CRB, we estimated that a net deposition of $9.40\,\mathrm{Tg\,yr^{-1}}$ (CI = 3.0, 16) occurred along the mainstem of the Congo River between the cities of Kisangani and Kinshasa. Hypothesizing that the net deposition of sediment occurred within the Cuvette Centrale thanks to its flat terrain and low flow velocities, we showed that sediment yield decreased within the Cuvette Centrale. Moreover, we highlighted a crucial lack of understanding of sediment dynamics occurring along the Congo River, as previous published estimates of net sediment deposition ranged from $2.53\,\mathrm{Tg\,yr^{-1}}$ to $23\,\mathrm{Tg\,yr^{-1}}$, which reflect a poor constraint on deposition rates.

By monitoring a globally significant but understudied tropical basin—i.e., the Congo River—these results contribute to understanding the source-to-sink transport of sediment in a globally significant but understudied tropical basin. By monitoring fluvial sediment transport, we aimed to provide a better understanding of the Earth-surface processes occurring within this watershed. Moreover, in the Congolese context of intense land-use change linked to a demographic expansion, we provided a baseline assessment of the sediment cycle, bringing to light a better knowledge of the sediment cycle which is necessary for anticipating its anthropogenically-driven modification to sediment and carbon regimes.

Code availability. All code used for generating the data in this paper will be made available before publication.

370 *Author contributions.* Conceptualization, K.V.O., N.C, P.Z., T.W.D., J.S. and J.D.H.; methodology, N.C and K.V.O.; software, N.C.; validation, N.C.; formal analysis, N.C.; investigation, N.C., K.V.O., and J.S.; resources, K.V.O.; data curation, N.C., M.B., T.W.D, L.W.D., J.D.H, J.N.W; writing—original draft preparation, N.C.; writing—review and editing, M.B., A.D.C, L.W.D, T.W.D., J.D.H, Y.H., J.N.W., J.Z.M., P.Z., J.S., and K.V.O.; visualization, N.C.; supervision, K.V.O and J.S.; project administration, J.S., K.V.O., J.D.H., and A.D.C.; funding acquisition, J.S., K.V.O. and J.D.H.

375 *Competing interests.* The authors have no competing interests to declare.

Acknowledgements. The authors thank Professor Steven Bouillon for sharing unpublished data from Kisangani, which form part of a larger dataset that has been collected thanks to the collaborative efforts of Ernest Tambwe, Alfred Toegaho, and Taylor Mambo (Centre de Surveillance de la Biodiviersité, Kisangani). This study is part of a project that has received funding from the Swiss National Science Foundation (SNSF) under the Sinergia project "Tropical Soil Erosion Dynamics (TropSEDs)" (CRSII5_205998).

References

Alsdorf, D., Beighley, E., Laraque, A., Lee, H., Tshimanga, R., O'Loughlin, F., Mahé, G., Dinga, B., Moukandi N'Kaya, G., and Spencer, R. G. M.: Opportunities for hydrologic research in the Congo Basin, Reviews of Geophysics, 54, 378–409, https://doi.org/10.1002/2016RG000517, 2016.

Balasubramanian, S. V., Pahlevan, N., Smith, B., Binding, C., Schalles, J., Loisel, H., Gurlin, D., Greb, S., Alikas, K., Randla, M., Bunkei, M., Moses, W., Nguyen, H., Lehmann, M. K., O'Donnell, D., Ondrusek, M., Han, T.-H., Fichot, C. G., Moore, T., and Boss, E.: Robust algorithm for estimating total suspended solids (TSS) in inland and nearshore coastal waters, Remote Sensing of Environment, 246, 111 768, https://doi.org/10.1016/j.rse.2020.111768, 2020.

Borrelli, P., Robinson, D. A., Fleischer, L. R., Lugato, E., Ballabio, C., Alewell, C., Meusburger, K., Modugno, S., Schütt, B., Ferro, V., Bagarello, V., Oost, K. V., Montanarella, L., and Panagos, P.: An assessment of the global impact of 21st century land use change on soil erosion, Nature Communications, 8, 2013, https://doi.org/10.1038/s41467-017-02142-7, 2017.

Bouillon, S., Yambélé, A., Spencer, R. G. M., Gillikin, D. P., Hernes, P. J., Six, J., Merckx, R., and Borges, A. V.: Organic matter sources, fluxes and greenhouse gas exchange in the Oubangui River (Congo River basin), Biogeosciences, 9, 2045–2062, https://doi.org/10.5194/bg-9-2045-2012, 2012.

Bouillon, S., Yambélé, A., Gillikin, D. P., Teodoru, C., Darchambeau, F., Lambert, T., and Borges, A. V.: Contrasting biogeochemical characteristics of the Oubangui River and tributaries (Congo River basin), Scientific Reports, 4, 5402, https://doi.org/10.1038/srep05402, 2014.

Cao, F., Tzortziou, M., Hu, C., Mannino, A., Fichot, C. G., Del Vecchio, R., Najjar, R. G., and Novak, M.: Remote sensing retrievals of colored dissolved organic matter and dissolved organic carbon dynamics in North American estuaries and their margins, Remote Sensing of Environment, 205, 151–165, https://doi.org/10.1016/j.rse.2017.11.014, 2018.

Center For International Earth Science Information Network: Gridded Population of the World, Version 4 (GPWv4): Population Density, Revision 11, https://doi.org/10.7927/H49C6VHW, 2017.

Coynel, A., Seyler, P., Etcheber, H., Meybeck, M., and Orange, D.: Spatial and seasonal dynamics of total suspended sediment and organic carbon species in the Congo River, Global Biogeochemical Cycles, 19, 2004GB002 335, https://doi.org/10.1029/2004GB002335, 2005.

Crezee, B., Dargie, G. C., Ewango, C. E. N., Mitchard, E. T. A., Emba B., O., Kanyama T., J., Bola, P., Ndjango, J.-B. N., Girkin, N. T., Bocko, Y. E., Ifo, S. A., Hubau, W., Seidensticker, D., Batumike, R., Imani, G., Cuní-Sanchez, A., Kiahtipes, C. A., Lebamba, J., Wotzka, H.-P., Bean, H., Baker, T. R., Baird, A. J., Boom, A., Morris, P. J., Page, S. E., Lawson, I. T., and Lewis, S. L.: Mapping peat thickness and carbon stocks of the central Congo Basin using field data, Nature Geoscience, 15, 639–644, https://doi.org/10.1038/s41561-022-00966-7, 2022.

Cutler, D. R., Edwards, T. C., Beard, K. H., Cutler, A., Hess, K. T., Gibson, J., and Lawler, J. J.: Random forests for classification in ecology, Ecology, 88, 2783–2792, https://doi.org/10.1890/07-0539.1, 2007.

Dargie, G. C., Lewis, S. L., Lawson, I. T., Mitchard, E. T. A., Page, S. E., Bocko, Y. E., and Ifo, S. A.: Age, extent and carbon storage of the central Congo Basin peatland complex, Nature, 542, 86–90, https://doi.org/10.1038/nature21048, 2017.

Datok, P., Sauvage, S., Fabre, C., Laraque, A., Ouillon, S., Moukandi N'kaya, G., and Sanchez-Perez, J.-M.: Sediment balance estimation of the 'Cuvette Centrale' of the Congo River Basin using the SWAT hydrological model, Water, 13, 1388, https://doi.org/10.3390/w13101388, 2021.

de Vente, J. and Poesen, J.: Predicting soil erosion and sediment yield at the basin scale: Scale issues and semi-quantitative models, Earth-Science Reviews, 71, 95–125, https://doi.org/10.1016/j.earscirev.2005.02.002, 2005.

de Vente, J., Poesen, J., Arabkhedri, M., and Verstraeten, G.: The sediment delivery problem revisited, Progress in Physical Geography: Earth and Environment, 31, 155–178, https://doi.org/10.1177/0309133307076485, 2007.

Dethier, E. N., Sartain, S. L., and Lutz, D. A.: Heightened levels and seasonal inversion of riverine suspended sediment in a tropical biodiversity hot spot due to artisanal gold mining, Proceedings of the National Academy of Sciences, 116, 23 936–23 941, https://doi.org/10.1073/pnas.1907842116, 2019.

Dethier, E. N., Renshaw, C. E., and Magilligan, F. J.: Toward improved accuracy of remote sensing approaches for quantifying suspended sediment: Implications for suspended-sediment monitoring, Journal of Geophysical Research: Earth Surface, 125, e2019JF005 033, https://doi.org/10.1029/2019JF005033, 2020.

Dethier, E. N., Renshaw, C. E., and Magilligan, F. J.: Rapid changes to global river suspended sediment flux by humans, Science, 376, 1447–1452, https://doi.org/10.1126/science.abn7980, 2022.

Doxaran, D., Froidefond, J.-M., and Castaing, P.: Remote-sensing reflectance of turbid sediment-dominated waters: Reduction of sediment type variations and changing illumination conditions effects by use of reflectance ratios, Applied Optics, 42, 2623, https://doi.org/10.1364/AO.42.002623, 2003.

Drake, T. W., Barthel, M., Mbongo, C. E., Mpambi, D. M., Baumgartner, S., Botefa, C. I., Bauters, M., Kurek, M. R., Spencer, R. G. M., McKenna, A. M., Haghipour, N., Ekamba, G. L., Wabakanghanzi, J. N., Eglinton, T. I., Van Oost, K., and Six, J.: Hydrology drives export and composition of carbon in a pristine tropical river, Limnology and Oceanography, 68, 2476–2491, https://doi.org/10.1002/lno.12436, 2023.

Fassoni-Andrade, A. C. and Paiva, R. C. D. D.: Mapping spatial-temporal sediment dynamics of river-floodplains in the Amazon, Remote Sensing of Environment, 221, 94–107, https://doi.org/10.1016/j.rse.2018.10.038, 2019.

Fick, S. E. and Hijmans, R. J.: WorldClim 2: new 1-km spatial resolution climate surfaces for global land areas, International Journal of Climatology, 37, 4302–4315, https://doi.org/10.1002/joc.5086, 2017.

Gardner, J., Pavelsky, T., Topp, S., Yang, X., Ross, M. R. V., and Cohen, S.: Human activities change suspended sediment concentration along rivers, Environmental Research Letters, 18, 064 032, https://doi.org/10.1088/1748-9326/acd8d8, 2023.

Georgiou, S., Mitchard, E. T. A., Crezee, B., Dargie, G. C., Young, D. M., Jovani-Sancho, A. J., Kitambo, B., Papa, F., Bocko, Y. E., Bola, P., Crabtree, D. E., Emba, O. B., Ewango, C. E. N., Girkin, N. T., Ifo, S. A., Kanyama, J. T., Mampouya, Y. E. W., Mbemba, M., Ndjango, J.-B. N., Palmer, P. I., Sjögersten, S., and Lewis, S. L.: Mapping water levels across a region of the Cuvette Centrale peatland complex, Remote Sensing, 15, 3099, https://doi.org/10.3390/rs15123099, 2023.

Gorelick, N., Hancher, M., Dixon, M., Ilyushchenko, S., Thau, D., and Moore, R.: Google Earth Engine: Planetary-scale geospatial analysis for everyone, Remote Sensing of Environment, 202, 18–27, https://doi.org/10.1016/j.rse.2017.06.031, 2017.

Grill, G., Lehner, B., Thieme, M., Geenen, B., Tickner, D., Antonelli, F., Babu, S., Borrelli, P., Cheng, L., Crochetiere, H., Ehalt Macedo, H., Filgueiras, R., Goichot, M., Higgins, J., Hogan, Z., Lip, B., McClain, M. E., Meng, J., Mulligan, M., Nilsson, C., Olden, J. D., Opperman, J. J., Petry, P., Reidy Liermann, C., Sáenz, L., Salinas-Rodríguez, S., Schelle, P., Schmitt, R. J. P., Snider, J., Tan, F., Tockner, K., Valdujo, P. H., Van Soesbergen, A., and Zarfl, C.: Mapping the world's free-flowing rivers, Nature, 569, 215–221, https://doi.org/10.1038/s41586-019-1111-9, 2019.

Han, B., Loisel, H., Vantrepotte, V., Mériaux, X., Bryère, P., Ouillon, S., Dessailly, D., Xing, Q., and Zhu, J.: Development of a semi-analytical algorithm for the retrieval of suspended particulate matter from remote sensing over clear to very turbid waters, Remote Sensing, 8, 211, https://doi.org/10.3390/rs8030211, 2016.

Hansen, M. C., Potapov, P. V., Moore, R., Hancher, M., Turubanova, S. A., Tyukavina, A., Thau, D., Stehman, S. V., Goetz, S. J., Loveland, T. R., Kommareddy, A., Egorov, A., Chini, L., Justice, C. O., and Townshend, J. R. G.: High-Resolution Global Maps of 21st-Century Forest Cover Change, Science, 342, 850–853, https://doi.org/10.1126/science.1244693, 2013.

Hemingway, J. D., Schefuß, E., Dinga, B. J., Pryer, H., and Galy, V. V.: Multiple plant-wax compounds record differential sources and ecosystem structure in large river catchments, Geochimica et Cosmochimica Acta, 184, 20–40, https://doi.org/10.1016/j.gca.2016.04.003, 2016.

Hemingway, J. D., Schefuß, E., Spencer, R. G., Dinga, B. J., Eglinton, T. I., McIntyre, C., and Galy, V. V.: Hydrologic controls on seasonal and inter-annual variability of Congo River particulate organic matter source and reservoir age, Chemical Geology, 466, 454–465, https://doi.org/10.1016/j.chemgeo.2017.06.034, 2017.

Hou, X., Xie, D., Feng, L., Shen, F., and Nienhuis, J. H.: Sustained increase in suspended sediments near global river deltas over the past two decades, Nature Communications, 15, 3319, https://doi.org/10.1038/s41467-024-47598-6, 2024.

HYBAM Observatory: Hybam – Amazon basin water resources observation service, https://hybam.obs-mip.fr/.

Kuhn, M.: Building predictive models in *R* using the **caret** package, Journal of Statistical Software, 28, https://doi.org/10.18637/jss.v028.i05, 2008.

Lal, R.: Soil erosion and the global carbon budget, Environment International, 29, 437–450, https://doi.org/10.1016/S0160-4120(02)00192-7, 2003.

Lambert, T., Bouillon, S., Darchambeau, F., Massicotte, P., and Borges, A. V.: Shift in the chemical composition of dissolved organic matter in the Congo River network, Biogeosciences, 13, 5405–5420, https://doi.org/10.5194/bg-13-5405-2016, 2016.

Langhorst, T. and Pavelsky, T.: Global observations of riverbank erosion and accretion from Landsat imagery, Journal of Geophysical Research: Earth Surface, 128, e2022JF006 774, https://doi.org/10.1029/2022JF006774, 2023.

Laraque, A., Bricquet, J. P., Pandi, A., and Olivry, J. C.: A review of material transport by the Congo River and its tributaries, Hydrological Processes, 23, 3216–3224, https://doi.org/10.1002/hyp.7395, 2009.

Laraque, A., Castellanos, B., Steiger, J., Lòpez, J. L., Pandi, A., Rodriguez, M., Rosales, J., Adèle, G., Perez, J., and Lagane, C.: A comparison of the suspended and dissolved matter dynamics of two large inter-tropical rivers draining into the Atlantic Ocean: the Congo and the Orinoco, Hydrological Processes, 27, 2153–2170, https://doi.org/10.1002/hyp.9776, 2013.

Lehner, B. and Grill, G.: Global river hydrography and network routing: baseline data and new approaches to study the world's large river systems, Hydrological Processes, 27, 2171–2186, https://doi.org/10.1002/hyp.9740, 2013.

Li, J., Wang, G., Song, C., Sun, S., Ma, J., Wang, Y., Guo, L., and Li, D.: Recent intensified erosion and massive sediment deposition in Tibetan Plateau rivers, Nature Communications, 15, 722, https://doi.org/10.1038/s41467-024-44982-0, 2024.

Libiseller, C. and Grimvall, A.: Performance of partial Mann–Kendall tests for trend detection in the presence of covariates, Environmetrics, 13, 71–84, https://doi.org/10.1002/env.507, 2002.

Liu, D., Bai, Y., He, X., Pan, D., Chen, C.-T. A., Li, T., Xu, Y., Gong, C., and Zhang, L.: Satellite-derived particulate organic carbon flux in the Changjiang River through different stages of the Three Gorges Dam, Remote Sensing of Environment, 223, 154–165, https://doi.org/10.1016/j.rse.2019.01.012, 2019.

Liu, M., Raymond, P. A., Lauerwald, R., Zhang, Q., Trapp-Müller, G., Davis, K. L., Moosdorf, N., Xiao, C., Middelburg, J. J., Bouwman, A. F., Beusen, A. H. W., Peng, C., Lacroix, F., Tian, H., Wang, J., Li, M., Zhu, Q., Cohen, S., Van Hoek, W. J., Li, Y., Li, Y., Yao, Y., and Regnier, P.: Global riverine land-to-ocean carbon export constrained by observations and multi-model assessment, Nature Geoscience, 17, 896–904, https://doi.org/10.1038/s41561-024-01524-z, 2024.

Ludwig, W., Probst, J., and Kempe, S.: Predicting the oceanic input of organic carbon by continental erosion, Global Biogeochemical Cycles, 10, 23–41, https://doi.org/10.1029/95GB02925, 1996.

Mariotti, A., Gadel, F., Giresse, P., and Kinga-Mouzeo: Carbon isotope composition and geochemistry of particulate organic matter in the Congo River (Central Africa): Application to the study of Quaternary sediments off the mouth of the river, Chemical Geology: Isotope Geoscience section, 86, 345–357, https://doi.org/10.1016/0168-9622(91)90016-P, 1991.

Martinez, J., Espinoza-Villar, R., Armijos, E., and Silva Moreira, L.: The optical properties of river and floodplain waters in the Amazon River Basin: Implications for satellite-based measurements of suspended particulate matter, Journal of Geophysical Research: Earth Surface, 120, 1274–1287, https://doi.org/10.1002/2014JF003404, 2015.

Martins, O. and Probst, J.-L.: Biogeochemistry of major African rivers: Carbon and minerals transport,, in: Biogeochemistry of major world rivers, edited by Degens, E. T., Kempe, S., and Richey, J. E., no. 42 in SCOPE, pp. 127–156, John Wiley & Sons, 1991.

McFeeters, S. K.: The use of the Normalized Difference Water Index (NDWI) in the delineation of open water features, International Journal of Remote Sensing, 17, 1425–1432, https://doi.org/10.1080/01431169608948714, 1996.

Moukandi N'kaya, G. D., Orange, D., Bayonne Padou, S. M., Datok, P., and Laraque, A.: Temporal variability of sediments, dissolved solids and dissolved organic matter fluxes in the Congo River at Brazzaville/Kinshasa, Geosciences, 10, 341, https://doi.org/10.3390/geosciences10090341, 2020.

Mushi, C., Ndomba, P., Trigg, M., Tshimanga, R., and Mtalo, F.: Assessment of basin-scale soil erosion within the Congo River Basin: A review, CATENA, 178, 64–76, https://doi.org/10.1016/j.catena.2019.02.030, 2019.

Mushi, C. A., Ndomba, P. M., Tshimanga, R. M., Trigg, M. A., Neal, J., Bola, G. B., Kabuya, P. M., Carr, A. B., Beya, J. T., Bates, P. D., and Mtalo, F.: Site selection, design, and implementation of a sediment sampling program on the Kasai River, a major tributary of the Congo River, in: Geophysical Monograph Series, edited by Tshimanga, R. M., N'kaya, G. D. M., and Alsdorf, D., pp. 427–446, Wiley, 1 edn., ISBN 978-1-119-65697-5 978-1-119-65700-2, https://doi.org/10.1002/9781119657002.ch22, 2022.

Narayanan, A., Cohen, S., and Gardner, J. R.: Riverine sediment response to deforestation in the Amazon basin, Earth Surface Dynamics, 12, 581–599, https://doi.org/10.5194/esurf-12-581-2024, 2024.

Novo, E. M. M., Hansom, J. D., and Curran†, P. J.: The effect of sediment type on the relationship between reflectance and suspended sediment concentration, International Journal of Remote Sensing, 10, 1283–1289, https://doi.org/10.1080/01431168908903967, 1989.

Novoa, S., Doxaran, D., Ody, A., Vanhellemont, Q., Lafon, V., Lubac, B., and Gernez, P.: Atmospheric corrections and multi-conditional algorithm for multi-sensor remote sensing of suspended particulate matter in low-to-high turbidity levels coastal waters, Remote Sensing, 9, 61, https://doi.org/10.3390/rs9010061, 2017.

Overeem, I., Hudson, B. D., Syvitski, J. P. M., Mikkelsen, A. B., Hasholt, B., Van Den Broeke, M. R., Noël, B. P. Y., and Morlighem, M.: Substantial export of suspended sediment to the global oceans from glacial erosion in Greenland, Nature Geoscience, 10, 859–863, https://doi.org/10.1038/ngeo3046, 2017.

Park, E. and Latrubesse, E. M.: Modeling suspended sediment distribution patterns of the Amazon River using MODIS data, Remote Sensing of Environment, 147, 232–242, https://doi.org/10.1016/j.rse.2014.03.013, 2014.

Pereira, L. S. F., Andes, L. C., Cox, A. L., and Ghulam, A.: Measuring suspended-sediment concentration and turbidity in the Middle Mississippi and Lower Missouri Rivers using Landsat data, JAWRA Journal of the American Water Resources Association, 54, 440–450, https://doi.org/10.1111/1752-1688.12616, 2018.

Peterson, K., Sagan, V., Sidike, P., Cox, A., and Martinez, M.: Suspended sediment concentration estimation from Landsat Imagery along the Lower Missouri and Middle Mississippi Rivers using an extreme learning machine, Remote Sensing, 10, 1503, https://doi.org/10.3390/rs10101503, 2018.

Poggio, L., De Sousa, L. M., Batjes, N. H., Heuvelink, G. B. M., Kempen, B., Ribeiro, E., and Rossiter, D.: SoilGrids 2.0: producing soil information for the globe with quantified spatial uncertainty, SOIL, 7, 217–240, https://doi.org/10.5194/soil-7-217-2021, 2021.

Potapov, P. V., Turubanova, S. A., Hansen, M. C., Adusei, B., Broich, M., Altstatt, A., Mane, L., and Justice, C. O.: Quantifying forest cover loss in Democratic Republic of the Congo, 2000–2010, with Landsat ETM+ data, Remote Sensing of Environment, 122, 106–116, https://doi.org/10.1016/j.rse.2011.08.027, 2012.

R Core Team: R: A Language and Environment for Statistical Computing, R Foundation for Statistical Computing, Vienna, Austria, https://www.R-project.org/, 2024.

Regnier, P., Friedlingstein, P., Ciais, P., Mackenzie, F. T., Gruber, N., Janssens, I. A., Laruelle, G. G., Lauerwald, R., Luyssaert, S., Andersson, A. J., Arndt, S., Arnosti, C., Borges, A. V., Dale, A. W., Gallego-Sala, A., Goddéris, Y., Goossens, N., Hartmann, J., Heinze, C., Ilyina, T., Joos, F., LaRowe, D. E., Leifeld, J., Meysman, F. J. R., Munhoven, G., Raymond, P. A., Spahni, R., Suntharalingam, P., and Thullner, M.: Anthropogenic perturbation of the carbon fluxes from land to ocean, Nature Geoscience, 6, 597–607, https://doi.org/10.1038/ngeo1830, 2013.

Runge, J.: The Congo River, Central Africa, in: Large Rivers, edited by Gupta, A., pp. 293–309, Wiley, 1 edn., ISBN 978-0-470-84987-3 978-0-470-72372-2, https://doi.org/10.1002/9780470723722.ch14, 2007.

Sagan, V., Peterson, K. T., Maimaitijiang, M., Sidike, P., Sloan, J., Greeling, B. A., Maalouf, S., and Adams, C.: Monitoring inland water quality using remote sensing: potential and limitations of spectral indices, bio-optical simulations, machine learning, and cloud computing, Earth-Science Reviews, 205, 103 187, https://doi.org/10.1016/j.earscirev.2020.103187, 2020.

Spencer, R. G., Hernes, P. J., Aufdenkampe, A. K., Baker, A., Gulliver, P., Stubbins, A., Aiken, G. R., Dyda, R. Y., Butler, K. D., Mwamba, V. L., Mangangu, A. M., Wabakanghanzi, J. N., and Six, J.: An initial investigation into the organic matter biogeochemistry of the Congo River, Geochimica et Cosmochimica Acta, 84, 614–627, https://doi.org/10.1016/j.gca.2012.01.013, 2012.

Spencer, R. G. M., Hernes, P. J., Dinga, B., Wabakanghanzi, J. N., Drake, T. W., and Six, J.: Origins, seasonality, and fluxes of organic matter in the Congo River, Global Biogeochemical Cycles, 30, 1105–1121, https://doi.org/10.1002/2016GB005427, 2016.

Sun, X., Tian, L., Fang, H., Walling, D. E., Huang, L., Park, E., Li, D., Zheng, C., and Feng, L.: Changes in global fluvial sediment concentrations and fluxes between 1985 and 2020, Nature Sustainability, 8, 142–151, https://doi.org/10.1038/s41893-024-01476-7, 2025.

Syvitski, J. and Milliman, J.: Geology, geography, and humans battle for dominance over the delivery of fluvial sediment to the coastal ocean, The Journal of Geology, 115, 1–19, https://doi.org/10.1086/509246, 2007.

Syvitski, J., Ángel, J. R., Saito, Y., Overeem, I., Vörösmarty, C. J., Wang, H., and Olago, D.: Earth's sediment cycle during the Anthropocene, Nature Reviews Earth & Environment, 3, 179–196, https://doi.org/10.1038/s43017-021-00253-w, 2022.

Syvitski, J. P. M., Vörösmarty, C. J., Kettner, A. J., and Green, P.: Impact of humans on the flux of terrestrial sediment to the global coastal ocean, Science, 308, 376–380, https://doi.org/10.1126/science.1109454, 2005.

Tian, S., Sha, A., Luo, Y., Ke, Y., Spencer, R., Hu, X., Ning, M., Zhao, Y., Deng, R., Gao, Y., Liu, Y., and Li, D.: A novel framework for river organic carbon retrieval through satellite data and machine learning, ISPRS Journal of Photogrammetry and Remote Sensing, 221, 109–123, https://doi.org/10.1016/j.isprsjprs.2025.01.028, 2025.

Topp, S. N., Pavelsky, T. M., Jensen, D., Simard, M., and Ross, M. R. V.: Research trends in the use of remote sensing for inland water quality science: Moving towards multidisciplinary applications, Water, 12, 169, https://doi.org/10.3390/w12010169, 2020.

Tshimanga, R. M., Trigg, M. A., Neal, J., Ndomba, P. M., Hughes, D. A., Carr, A. B., Kabuya, P. M., Bola, G. B., Mushi, C. A., Beya, J. T., Ngandu, F. K., Mokango, G. M., Mtalo, F., and Bates, P. D.: New measurements of water dynamics and sediment transport along the middle reach of the Congo River and the Kasai Tributary, in: Geophysical Monograph Series, edited by Tshimanga, R. M., Moukandi N'kaya, G. D., and Alsdorf, D., pp. 447–467, Wiley, 1 edn., ISBN 978-1-119-65697-5 978-1-119-65700-2, https://doi.org/10.1002/9781119657002.ch23, 2022.

United Nations Department of Economic and Social Affairs: World Population Prospects 2024: Summary of Results, United Nations, Erscheinungsort nicht ermittelbar, ISBN 978-92-1-106513-8, 2024.

Van Oost, K. and Six, J.: Reconciling the paradox of soil organic carbon erosion by water, Biogeosciences, 20, 635–646, https://doi.org/10.5194/bg-20-635-2023, 2023.

Wager, S., Hastie, T., and Efron, B.: Confidence intervals for random forests: The jackknife and the infinitesimal jackknife, Journal of Machine Learning Research, 15, 1625–1651, http://jmlr.org/papers/v15/wager14a.html, 2014.

Walling, D.: The sediment delivery problem, Journal of Hydrology, 65, 209–237, https://doi.org/10.1016/0022-1694(83)90217-2, 1983.

Walling, D. and Fang, D.: Recent trends in the suspended sediment loads of the world's rivers, Global and Planetary Change, 39, 111–126, https://doi.org/10.1016/S0921-8181(03)00020-1, 2003.

Walling, D. E.: Linking land use, erosion and sediment yields in river basins, Hydrobiologia, 410, 223–240, https://doi.org/10.1023/A:1003825813091, 1999.

Wang, J., Lu, X. X., Liew, S. C., and Zhou, Y.: Retrieval of suspended sediment concentrations in large turbid rivers using Landsat ETM+: An example from the Yangtze River, China, Earth Surface Processes and Landforms, 34, 1082–1092, https://doi.org/10.1002/esp.1795, 2009.

Wongchuig, S., Kitambo, B., Papa, F., Paris, A., Fleischmann, A. S., Gal, L., Boucharel, J., Paiva, R., Oliveira, R. J., Tshimanga, R. M., and Calmant, S.: Improved modeling of Congo's hydrology for floods and droughts analysis and ENSO teleconnections, Journal of Hydrology: Regional Studies, 50, 101 563, https://doi.org/10.1016/j.ejrh.2023.101563, 2023.

Wright, M. N. and Ziegler, A.: **ranger** : A fast implementation of random forests for high dimensional data in *C++* and *R*, Journal of Statistical Software, 77, https://doi.org/10.18637/jss.v077.i01, 2017.

Xu, L., Saatchi, S. S., Shapiro, A., Meyer, V., Ferraz, A., Yang, Y., Bastin, J.-F., Banks, N., Boeckx, P., Verbeeck, H., Lewis, S. L., Muanza, E. T., Bongwele, E., Kayembe, F., Mbenza, D., Kalau, L., Mukendi, F., Ilunga, F., and Ebuta, D.: Spatial Distribution of Carbon Stored in Forests of the Democratic Republic of Congo, Scientific Reports, 7, 15 030, https://doi.org/10.1038/s41598-017-15050-z, 2017.

Yepez, S., Laraque, A., Martinez, J.-M., De Sa, J., Carrera, J. M., Castellanos, B., Gallay, M., and Lopez, J. L.: Retrieval of suspended sediment concentrations using Landsat-8 OLI satellite images in the Orinoco River (Venezuela), Comptes Rendus. Géoscience, 350, 20–30, https://doi.org/10.1016/j.crte.2017.08.004, 2017.

Zanaga, D., Van De Kerchove, R., Daems, D., De Keersmaecker, W., Brockmann, C., Kirches, G., Wevers, J., Cartus, O., Santoro, M., Fritz, S., Lesiv, M., Herold, M., Tsendbazar, N.-E., Xu, P., Ramoino, F., and Arino, O.: ESA WorldCover 10 m 2021 v200, https://doi.org/10.5281/ZENODO.7254221, 2022.

https://doi.org/10.5194/egusphere-2026-247
Preprint. Discussion started: 3 February 2026

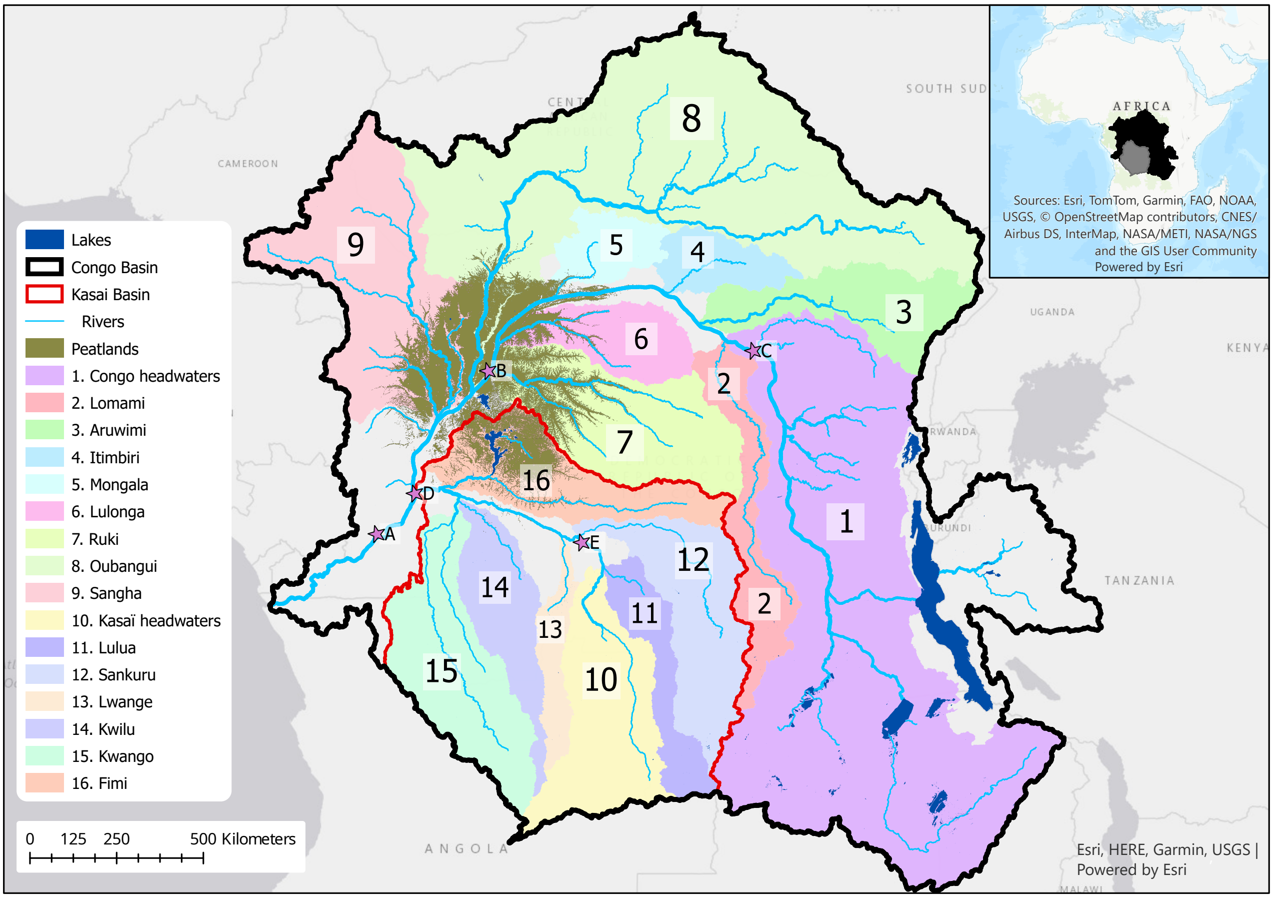

Sources: Esri, TomTom, Garmin, FAO, NOAA, USGS, © OpenStreetMap contributors, CNES/Airbus DS, InterMap, NASA/METI, NASA/NGS and the GIS User Community
Powered by Esri

Esri, HERE, Garmin, USGS | Powered by Esri

Figure 1. Map of the Congo Basin (black line), Kasaï Basin (red line), and their main tributaries (numbered 1-9 for Congo and 10-16 for Kasaï). The main fluvial network is in light blue, lakes are dark blue and the Cuvette Centrale peatland extent is in dark green (Crezee et al., 2022). Purple stars are the cities of A) Kinshasa-Brazzaville , B) Mbandaka, C) Kisangani, D) Kwamouth, and E) Ilebo.

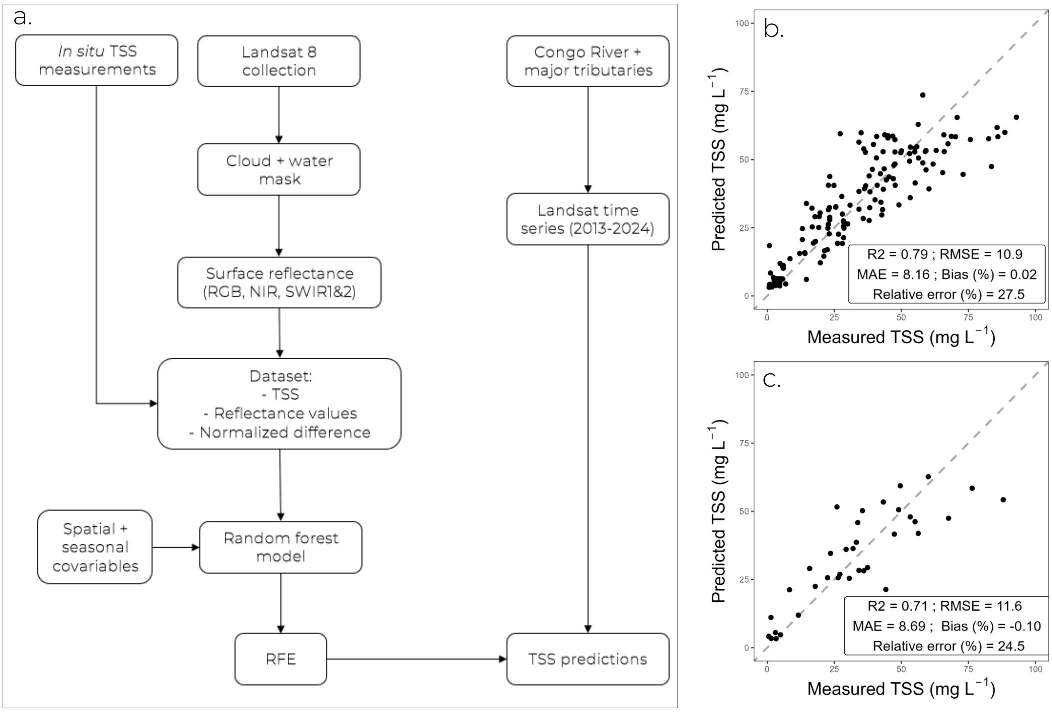

Figure 2. Satellite data collection and model calibration workflow (a), scatterplot of in situ measured TSS and predicted TSS for training data (b) and validation data (c). Dashed gray line in panels b. and c. is 1:1 line.

Table 1. Comparison of different RF model calibrations (training dataset, n = 148), with/without RFE, and with/without spatial and temporal covariables. The RF model used for all TSS predictions in this article is in italics.

	R^2	MAE ($mg\,L^{-1}$)	RMSE ($mg\,L^{-1}$)
RF (with covariables & RFE)	*0.79*	*8.15*	*10.9*
RF (no covariables & RFE)	0.76	8.61	11.5
RF (with covariables, no RFE)	0.78	8.29	11.1
RF (no covariables, with RFE)	0.77	8.52	11.5

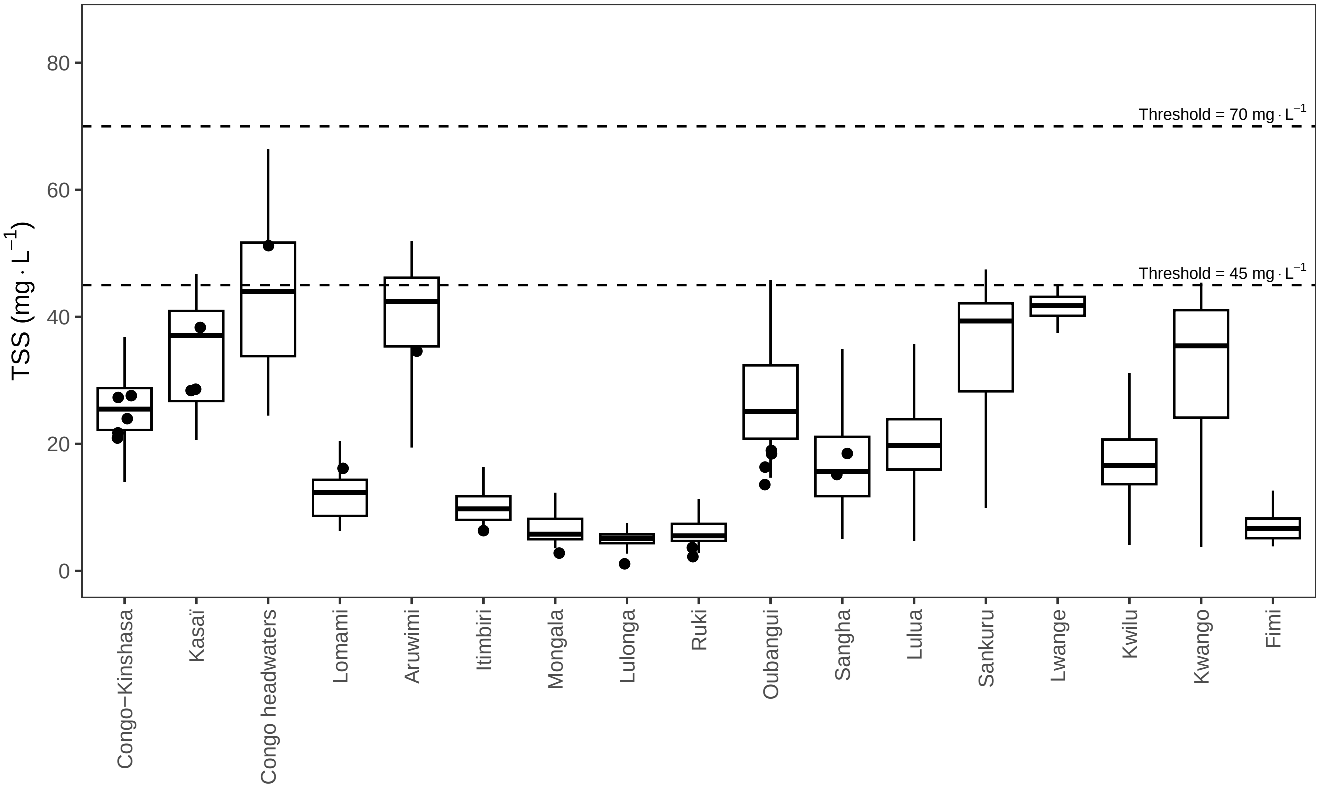

Figure 3. Boxplot of predicted TSS (2015-2019) in $\mathrm{mg\,L^{-1}}$ by basin outlet, where boxes are the quartile range, whiskers are the 5%-95% range (outliers not plotted) and the black bar is the median. Dots correspond to TSS time series means from the literature (Bouillon et al., 2012, 2014; Drake et al., 2023; Hemingway et al., 2016; HYBAM Observatory; Lambert et al., 2016; Laraque et al., 2009; Mariotti et al., 1991; Mushi et al., 2022; Spencer et al., 2016, and CSB monitoring), and dashed horizontal lines are hypothesized thresholds of spectral saturation in the prediction for $45\,\mathrm{mg\,L^{-1}}$ and $70\,\mathrm{mg\,L^{-1}}$.

https://doi.org/10.5194/egusphere-2026-247
Preprint. Discussion started: 3 February 2026

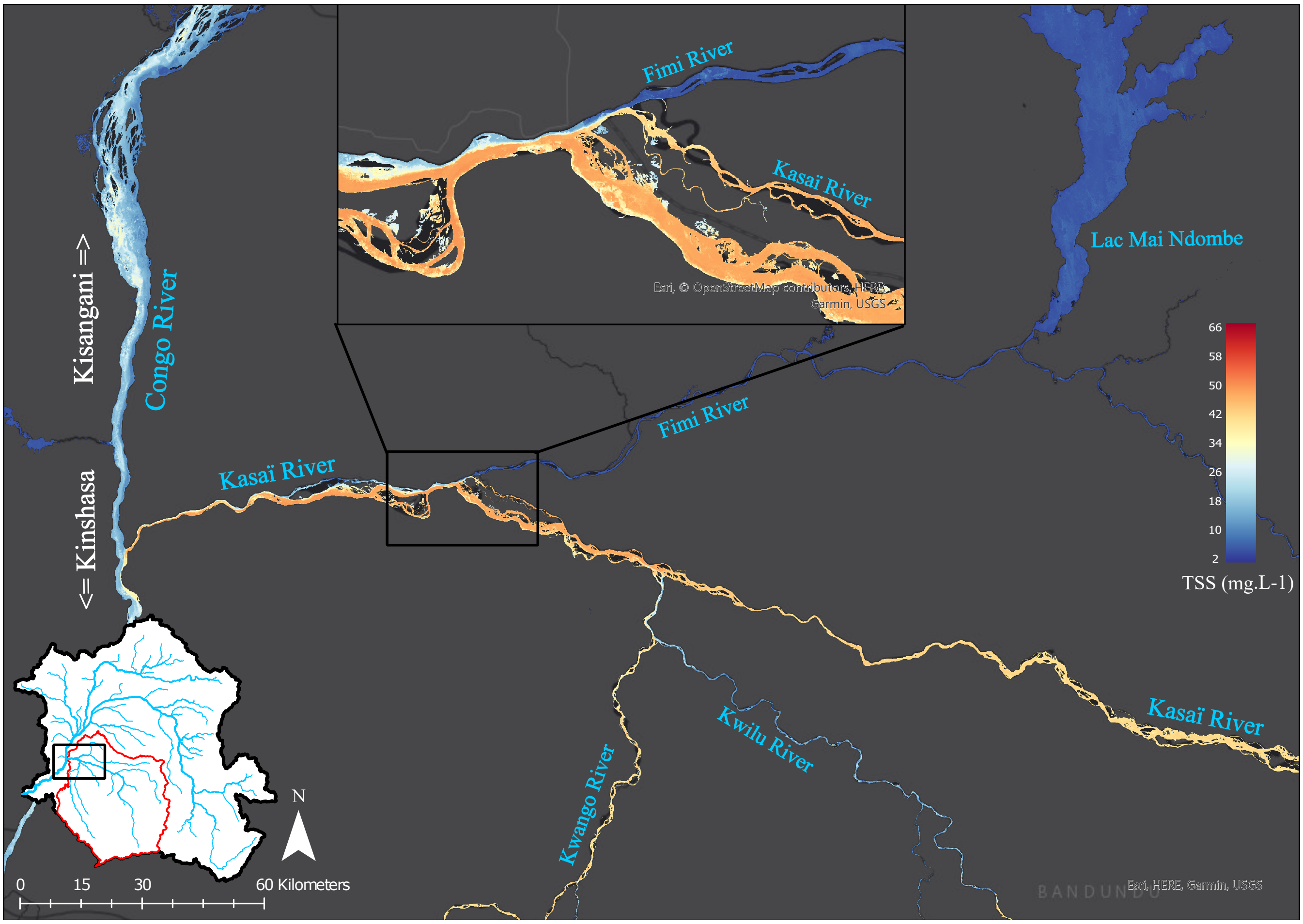

Figure 4. Gridded map of TSS ($\mathrm{mg\,L^{-1}}$) at the confluence of the Kasaï River with the Congo River. TSS predictions were based on reflectance data of “wet” season (September to April in Kinshasa) 2018-2020 summarized as the median pixels’ reflectance. Higher TSS values are in red, while lower TSS values are in blue. River names are in light blue text, while white text and arrows correspond to direction towards major cities along the Congo River.

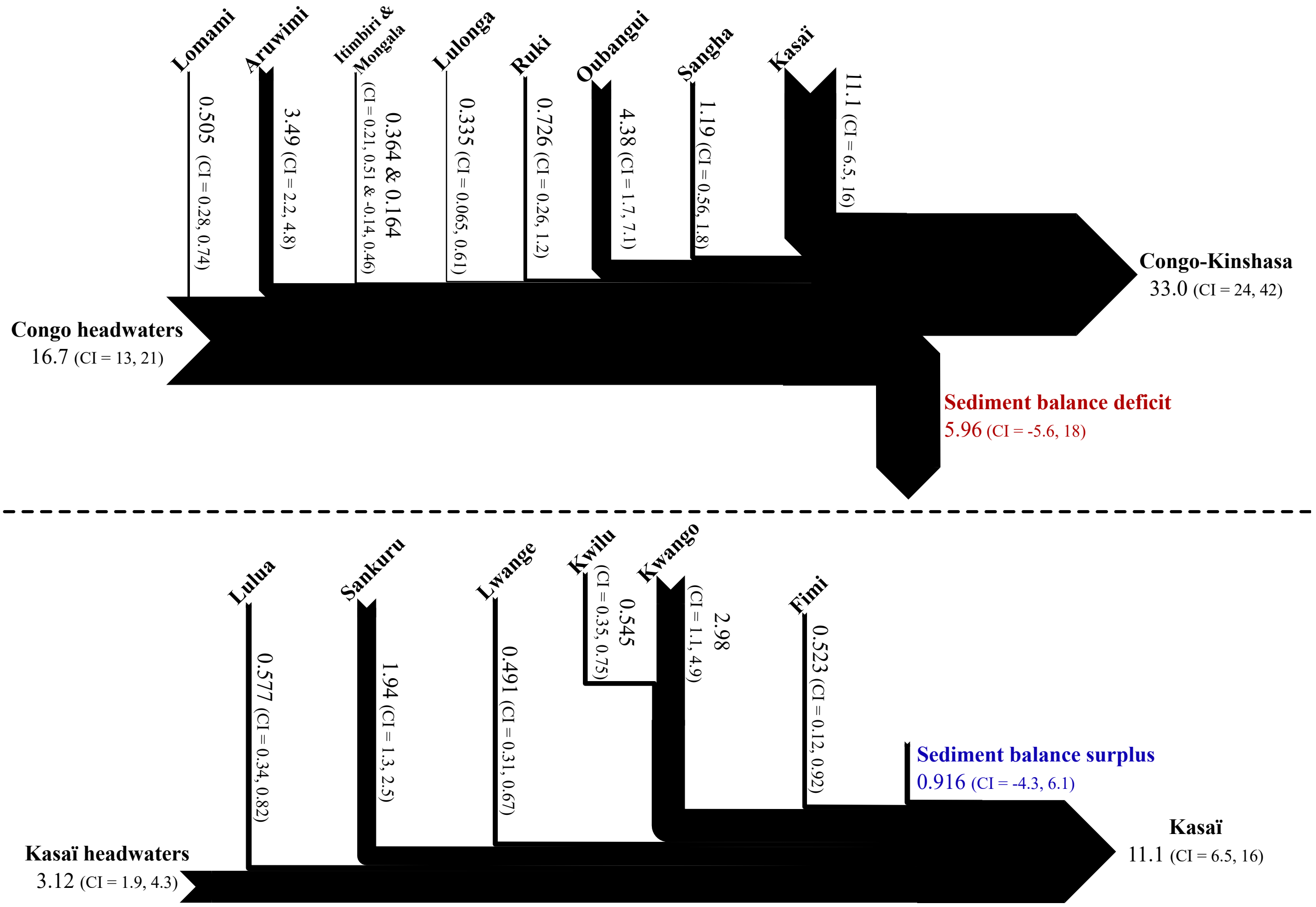

Figure 5. Median sediment yield budgets (Tg yr^{-1}) for the Congo River Basin (a) and the Kasaï River Basin (b) from 2015-2019. Sediment balance deficit (red) signified that the inputs (headwaters and tributaries) were higher than the output while a sediment balance surplus (blue) signified that the output was higher than the sum of all inputs. The size of lines for each component are proportional to sediment yield.

https://doi.org/10.5194/egusphere-2026-247
Preprint. Discussion started: 3 February 2026

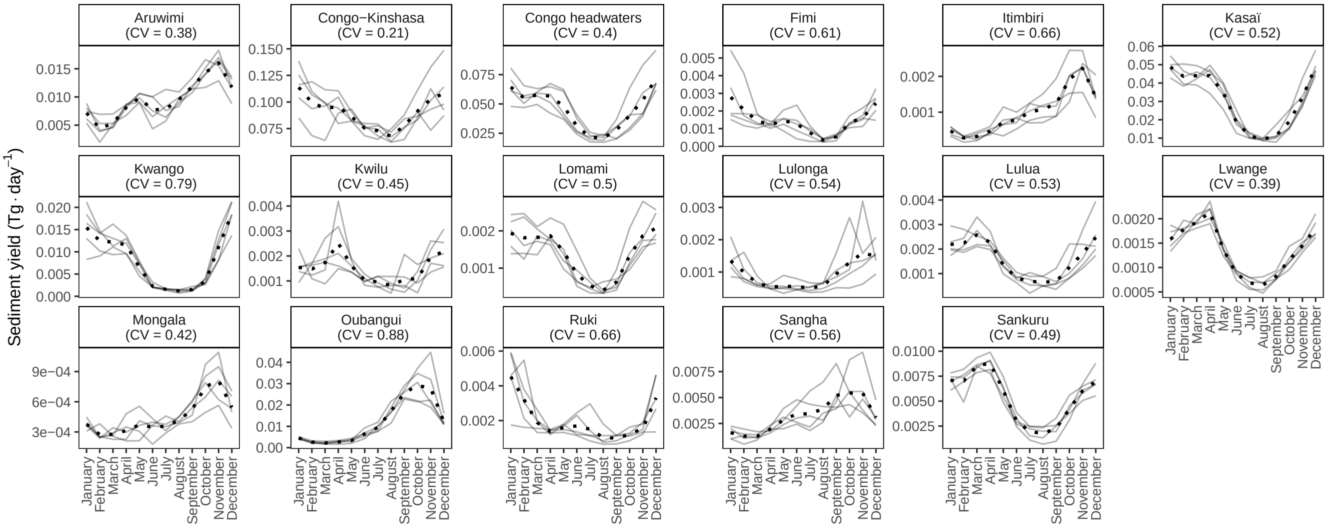

Figure 6. Line plot of daily sediment yield evolution ($\mathrm{Tg\,yr^{-1}}$) from 2015-2019 (individual gray lines for each year), for each basin. Dotted black lines are mean sediment yield, and CV is mean yearly coefficient of variation for each basin.

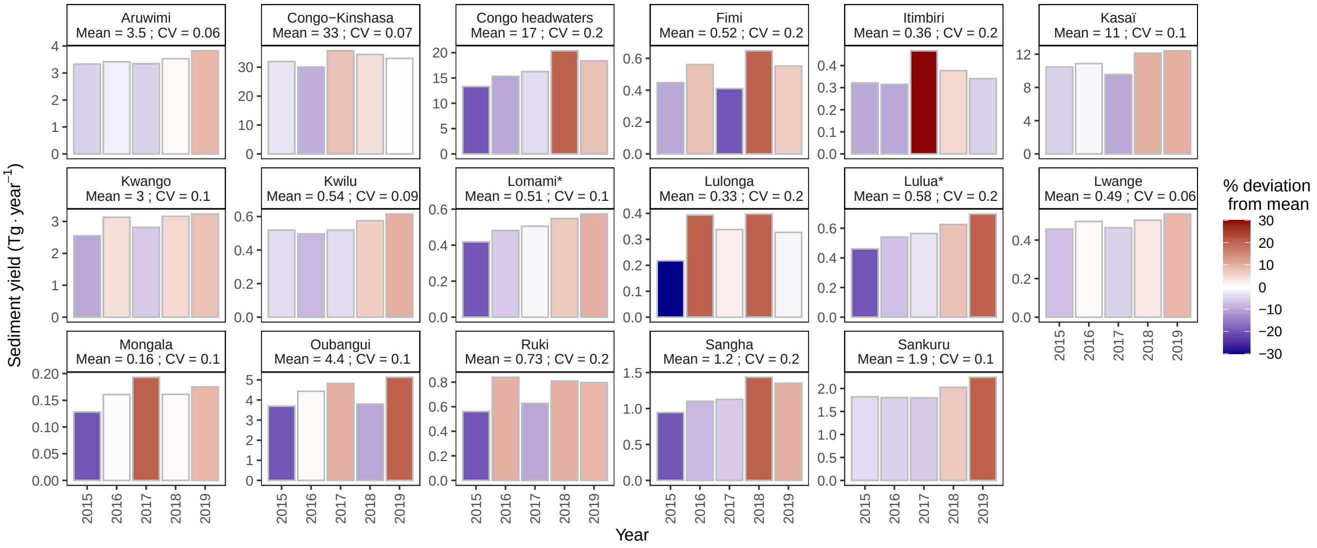

Figure 7. Barplot of sediment yield evolution ($\mathrm{Tg\,yr^{-1}}$) for each year from 2015 to 2019 for each basin (stars next to basin name signify a statistically significant monotonic evolution). Mean is the mean sediment yield of all years, CV is the coefficient of variation of yearly sediment yields and bars are colored by % deviation from each basin's mean (red is positive difference and blue is negative difference from mean).

https://doi.org/10.5194/egusphere-2026-247
Preprint. Discussion started: 3 February 2026

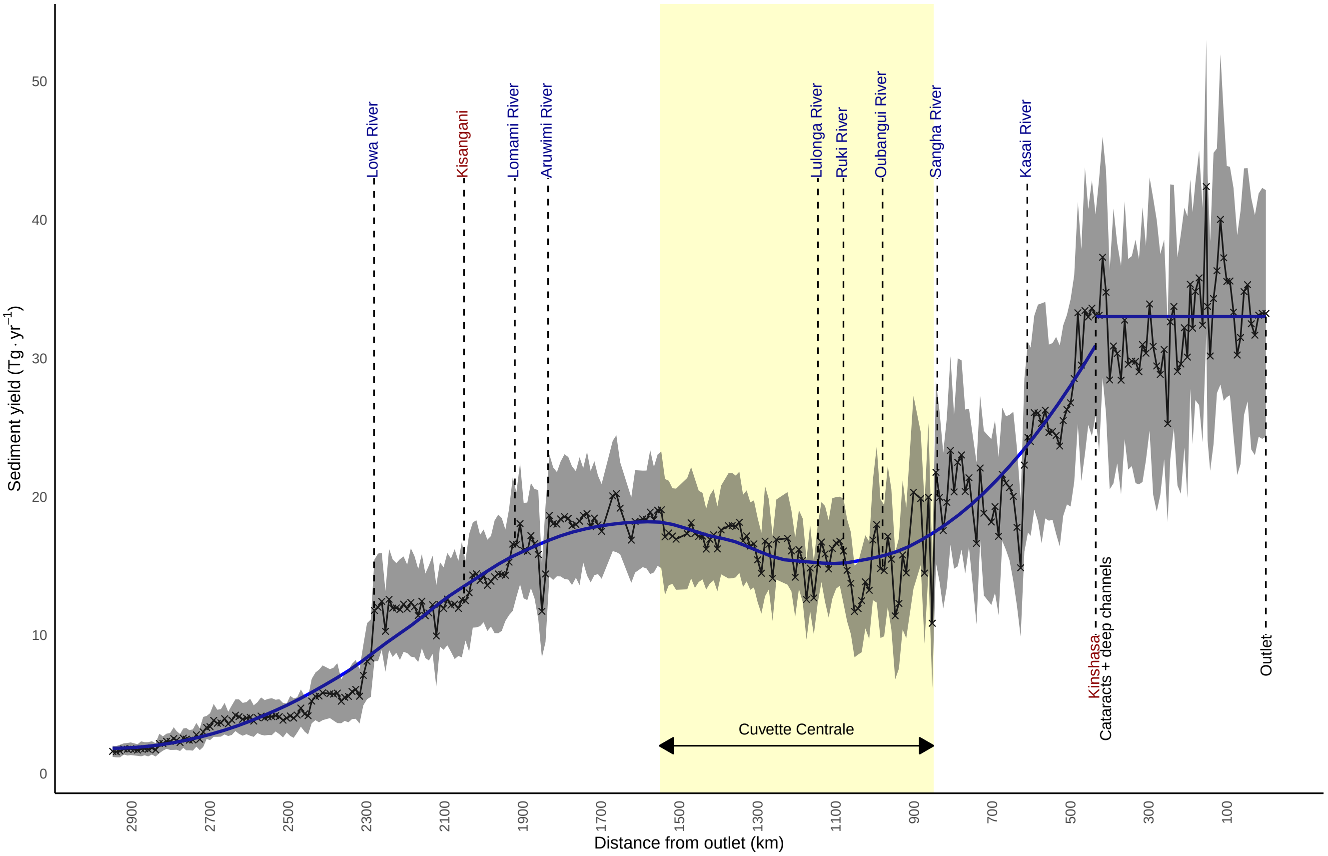

Figure 8. Evolution of yearly sediment yields ($\mathrm{Tg\,yr^{-1}}$) along the Congo River mainstem as a median from 2015-2019. River confluences are indicated in blue, cities in red, and notable sections in black text. Black crosses and line are predicted sediment yield, confidence interval in gray, and the blue line is smoothed sediment yield until Kinshasa (loess method), then mean sediment yield until the outlet. Yellow strip is the Cuvette Centrale.

Table 2. Median sediment yields from 2015-2019 (in $\mathrm{Tg\,yr^{-1}}$) compared to published literature. This study's results are written in bold. Note overlapping datasets from Moukandi N'kaya et al. (2020), Laraque et al. (2009), and Coynel et al. (2005). Rows are in italics when sampling station are different to ours, and a star signifies sediment yield was recomputed from the published dataset.

River	Sediment yield	Source	Sampling year
Congo-Kinshasa	**33.0**	**This study**	**2015-2019**
	48	Martins and Probst (1991)	1980-1981
	30.34	Moukandi N'kaya et al. (2020)	1987-1993
	30.7	Coynel et al. (2005)	1990-1993
	28.94	Laraque et al. (2009)	1993
	37.1	Datok et al. (2021)	2000-2012
	33	Laraque et al. (2013)	2006-2010
	34.41	Moukandi N'kaya et al. (2020)	2006-2017
	29.21	Spencer et al. (2016)	2009-2010
Oubangui	**4.38**	**This study**	**2015-2019**
	2.5	*Coynel et al. (2005)*	*1990-1996*
	2.72	*Laraque et al. (2009)*	*1993*
	1.5	*Datok et al. (2021)*	*2000-2012*
	2.45	*Bouillon et al. (2012)*	*2010-2011*
	1.63	*Bouillon et al. (2014)*	*2011-2012*
Sangha	**1.19**	**This study**	**2015-2019**
	1.0	*Coynel et al. (2005)*	*1991*
	1.64	*Laraque et al. (2009)*	*1993*
	0.94	*Datok et al. (2021)*	*2000-2012*
Kasaï	**11.1**	**This study**	**2015-2019**
	8.06	Laraque et al. (2009)	1993
	10.50	Datok et al. (2021)	2000-2012
Ruki	**0.726**	**This study**	**2015-2019**
	1.60	Datok et al. (2021)	2000-2012
	0.4*	Drake et al. (2023)	2019-2020
Upstream Congo	**16.7**	**This study**	**2015-2019**
	12.94	*Laraque et al. (2009)*	*1993*
	26.98	*Datok et al. (2021)*	*2000-2012*

Appendix A

A1 Time window choice

The time window of matches between in situ TSS observation and satellite spectral data was optimized thanks to repeated calibrations of an RF model with increasing time window (from 1-15 days) as well as keeping all matches without a limit on time window. Models were compared in terms of MAE, relative error, RMSE, and R^2, where the optimal time window maximized R^2 and minimized MAE, relative error, and RMSE (Fig. A1).

A2 Machine learning algorithm selection

Linear and machine learning algorithms were tuned and fit to the training dataset using spectral variables and 5 repetitions of a 10-fold cross-validation. Mean RMSE, MAE, R^2, and relative error, were computed and the algorithm with the lowest errors (RMSE) was selected. Algorithms, selected from the caret library (Kuhn, 2008), were a linear model (LM), support vector machines with linear kernel (SVML), support vector machines with polynomial kernel (SVMP), lasso and elastic-net regularized generalized linear models (GLMNET), multivariate adaptive regression spline (MARS), partial least squares regression (PLS), k-nearest neighbors regression (KNN), random forest (RF), extreme gradient boosting (XGBM), cubist regression (CUBIST), and stochastic gradient boosting (GBM). The RF algorithm had the lowest RMSE, MAE and relative error, and had the highest R^2 of all the algorithms (Fig. A5) and was therefore chosen for use in the prediction model.

A3 Discharge errors estimation

Daily discharge data for the entire Congo River Basin was acquired from a published dataset (Wongchuig et al., 2023), who used a combined approach of physical constraints (including satellite altimetry) and hydrological modelling to obtain a daily time series (1984-2020) of river discharge for large and small rivers throughout the basin. However, little information was provided on errors, so confidence intervals for the dataset were simulated, under the assumptions of a normal distribution of errors centered around 0, homoscedasticity, and that the Kling-Gupta Efficiency (KGE) was 0.84. This value was taken from Wongchuig et al. (2023) and it is the median value of their 6 independent validations (i.e., comparisons to in situ time series). The KGE was chosen as the error parameter with the least amount of variation between the different validations.

For each virtual monitoring station, a time series was extracted. From that time series, a new dataset was simulated with a random normal distribution for each data point. These normal distributions had a size of 10,000, and they were centered around the observation point. The spread of the distribution (i.e., its standard deviation) was optimized to obtain a KGE of 0.84 between the time series and the entire simulated data. Finally, for each observation, the normal distribution's 2.5% and 97.5% quantiles were taken as the confidence interval.

https://doi.org/10.5194/egusphere-2026-247
Preprint. Discussion started: 3 February 2026

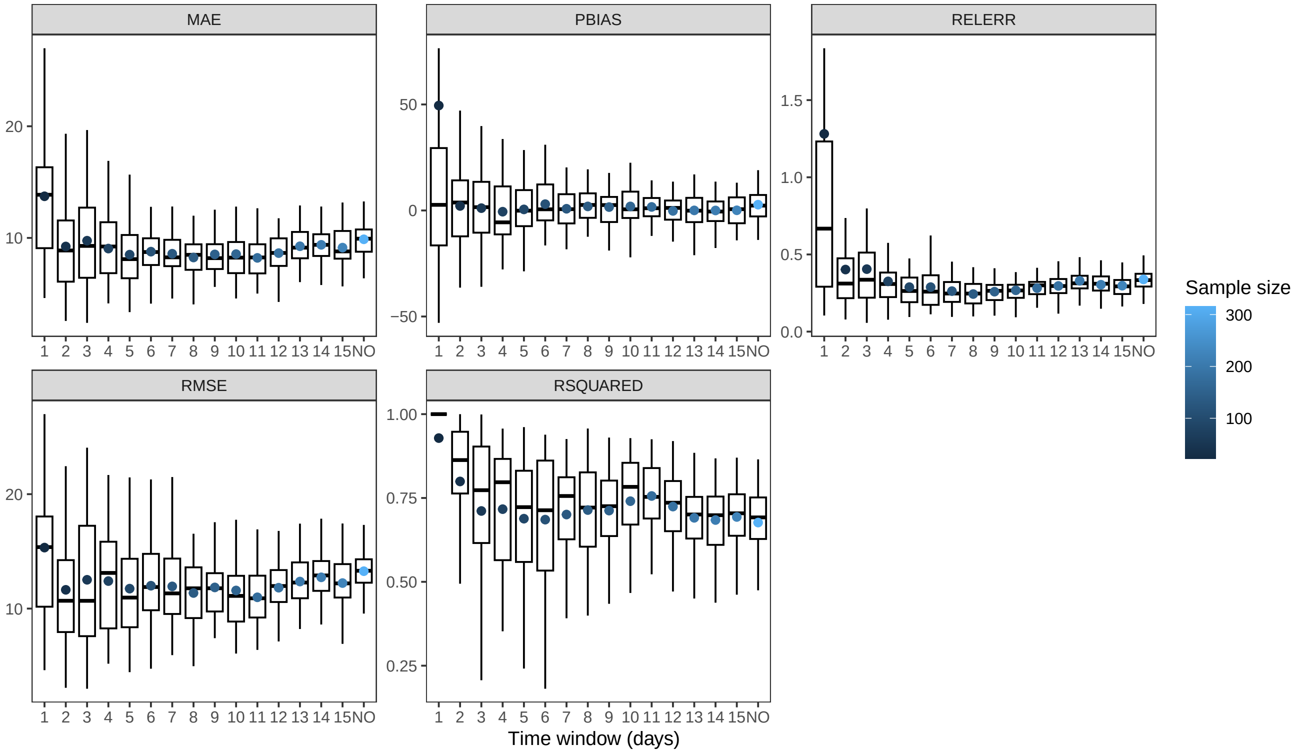

Figure A1. Accuracy of RF model calibration using increasing time windows for matches between in situ observation and satellite spectral data (1-15 days and no time window limit) for MAE ($\mathrm{mg\,L^{-1}}$), percent bias (PBIAS, %), relative error (RELERR), RMSE ($\mathrm{mg\,L^{-1}}$) and R^2 (RSQUARED). Box-and-whisker plots correspond to the cross-validation for the quartile of errors (boxes) and 5%-95% percentile (whiskers) (values outside 5-95% range were not plotted), while colored dots are the mean of the error, colored by the sample size upon which the model was calibrated.

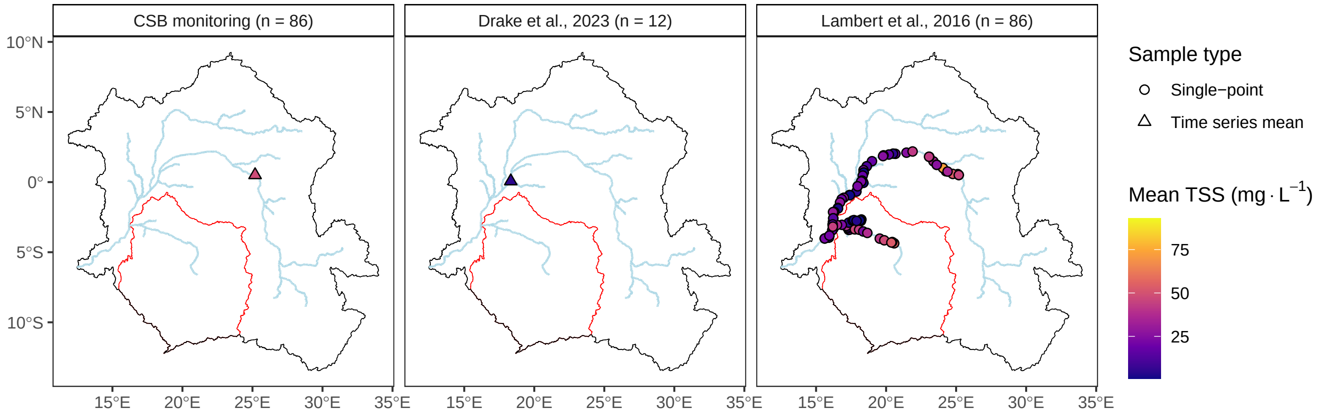

Figure A2. Maps of in situ sample locations which were used in the calibration of the RF model, where each map of the Congo Basin (black outline) and Kasaï Basin (red outline) corresponds to each data source (n = the number of observations used in each dataset). Triangles signify a time series whereas circles signify single point sampling. Triangles were colored by mean TSS ($\mathrm{mg\,L^{-1}}$) and circles were colored by single TSS value. Blue lines represent the main river network of the Congo River Basin.

https://doi.org/10.5194/egusphere-2026-247
Preprint. Discussion started: 3 February 2026

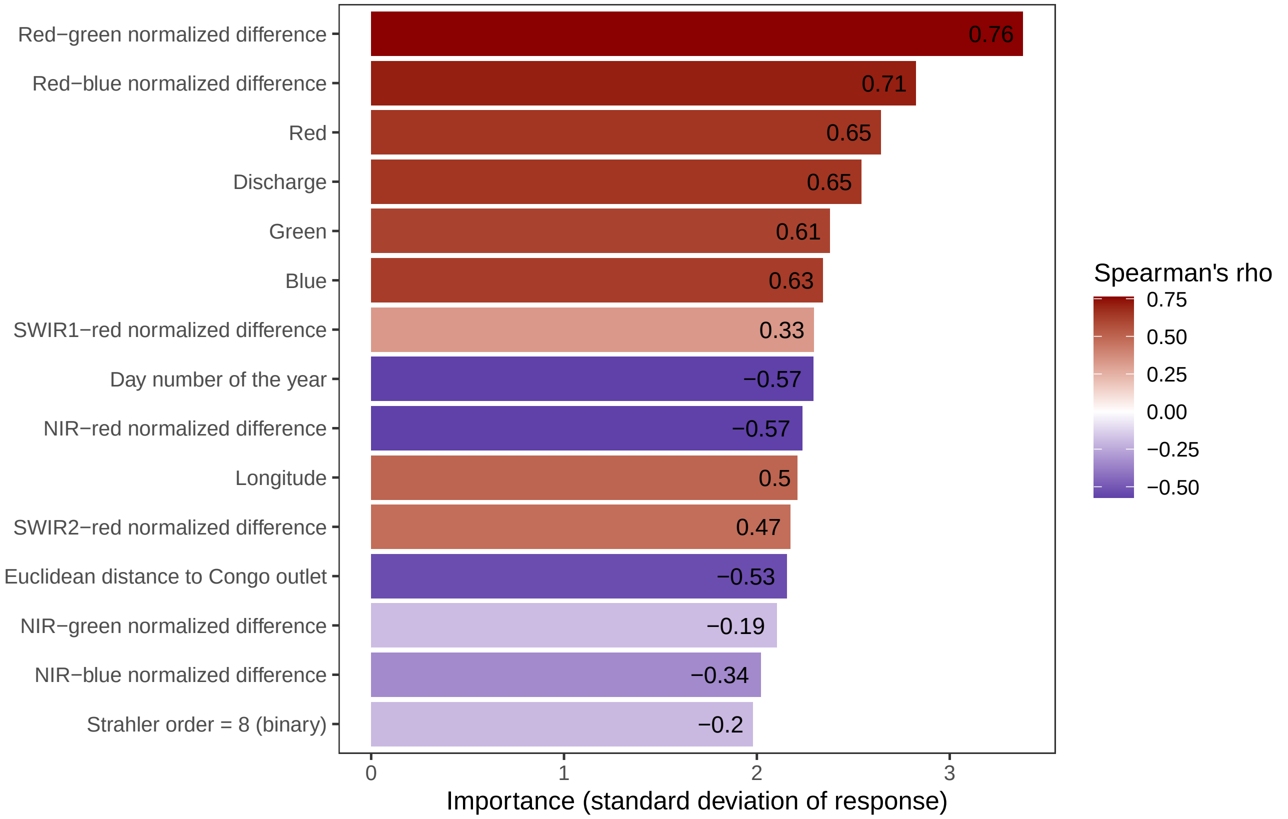

Figure A3. Barplot of variable importance (standard deviation of the response of the variable in the model), ordered from most important (highest standard deviation) on top to least important at the bottom. Colors (red positive, blue negative) and numbers correspond to the correlation (Spearman's rho) between TSS and corresponding variable.

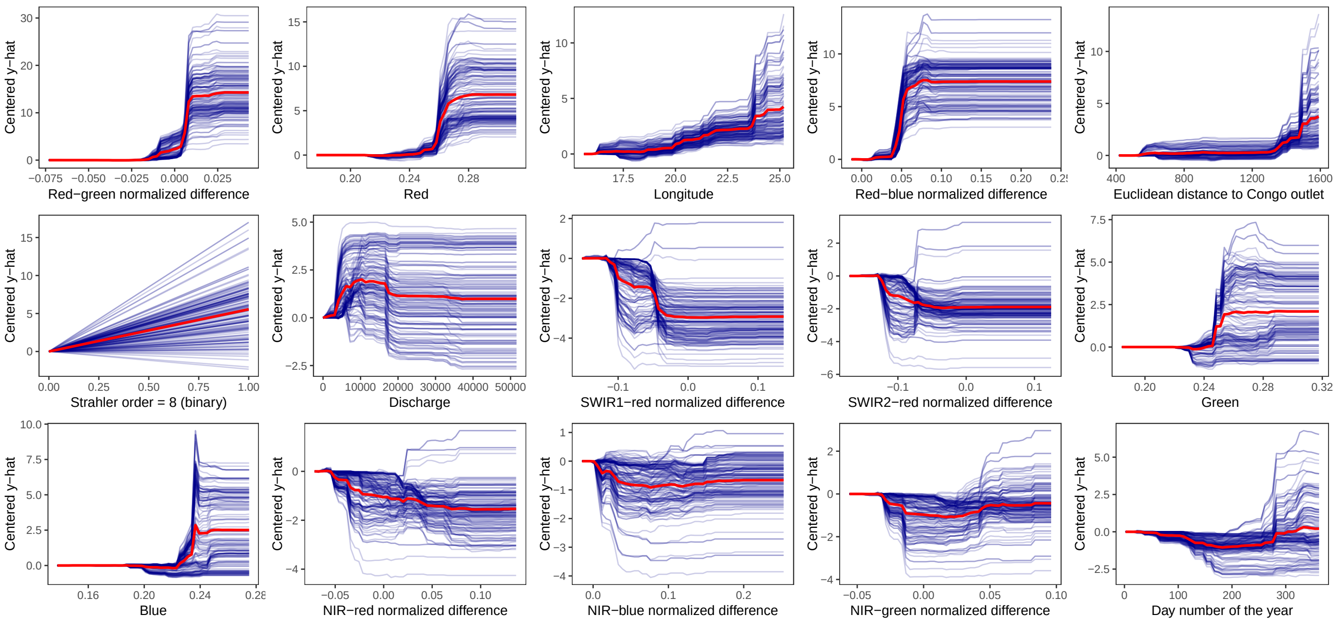

Figure A4. Partial dependence plots of variables included in our random forest model, where the horizontal axis corresponds to each variable's range of values and the vertical axis (centered y-hat) is the response of the RF model to the evolution of each variable. The blue lines are response curves for each individual observation of the training dataset, and the red line is the mean of all responses curves.

https://doi.org/10.5194/egusphere-2026-247
Preprint. Discussion started: 3 February 2026

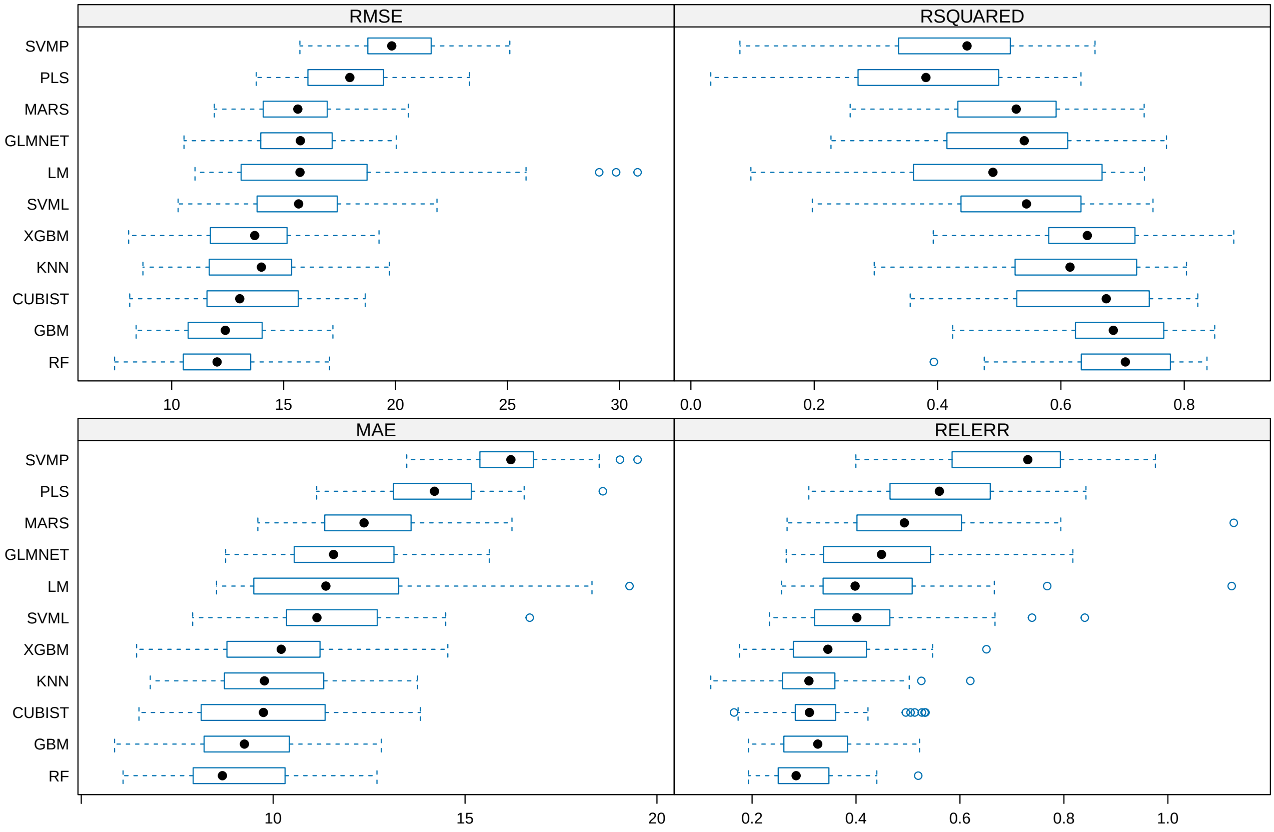

Figure A5. Boxplots of model calibration accuracy (cross-validation of calibration yielded interquartile range as a box, 5%-95% quantiles for the whiskers, blue circles for outliers (outside 5-95% quanrtile range), and black dots as mean) for TSS. Accuracy is measured as RMSE ($\mathrm{mg\,L^{-1}}$), R^2 (RSQUARED), MAE ($\mathrm{mg\,L^{-1}}$), and relative error (RELERR). Algorithms which were tested are a linear model (LM), support vector machines with linear kernel (SVML), support vector machines with polynomial kernel (SVMP), lasso and elastic-net regularized generalized linear models (GLMNET), multivariate adaptive regression spline (MARS), partial least squares regression (PLS), k-nearest neighbors regression (KNN), random forest (RF), extreme gradient boosting (XGBM), cubist regression (CUBIST), and stochastic gradient boosting (GBM). Algorithms are sorted by increasing median RMSE (top is highest and bottom is lowest).